American Mineralogist, Volume 67, pages 975–996, 1982

The anorthoclase structures: the effects of temperature and composition

GEORGE E. HARLOW

Department of Mineral Sciences
American Museum of Natural History
New York, New York 10024

Abstract

Cell-parameter and structure refinements using single-crystal X-ray diffraction have been carried out on three natural low-Ca anorthoclases (K–analbites), ($Or_{32.5}Ab_{66.7}An_{0.8}$, $Or_{22.3}Ab_{70.8}An_{6.9}$, $Or_{13.8}Ab_{83.7}An_{2.5}$), at room temperature and at temperatures above the triclinic/monoclinic symmetry inversion (400°, 510°, and 750° C, respectively). Room temperature cell parameters are consistent with monoclinic Si,Al topochemistry and a high degree of disorder (t_1 = 0.50 to 0.52 from the *b*–*c* plot). A room-temperature inversion composition of Or_{36} is extrapolated from $\cos^2\alpha^*$ and T–O–T angle plots. Mean M–O bond lengths and T–O–T angles increase with potassium content, whereas their variances decrease, indicating a trend to more regular coordination, as in sanidine. A similar relationship develops with thermal expansion and the structural changes associated with inversion to monoclinic symmetry, but the individual ⟨M–O⟩ values suggest a non-isotropic, ellipsoidal expansion of Na-rich alkali cavities. Examination of dimensional change in the structures due to change in temperature and alkali composition indicates that most of the effect is related to change in M–O bonding, with the aluminosilicate framework responding passively. Anisotropic thermal models for single M sites produce non-positive definite ellipsoids. Modeling with isotropic split-sites yields four parts for the more sodic structures, essentially identical to the models for high albite or analbite. For the more potassic crystals, a separate isotropic K site and an anisotropic Na(Ca) site is indicated.

Introduction

There is much interest in characterizing the variation in the feldspar structures because of the abundance and importance of feldspars in petrologic processes and because of their general significance in mineralogical studies of exsolution and polymorphism, especially order–disorder. The structures of disordered alkali feldspars with near end-member compositions have been widely studied. Sanidine, a monoclinic (*C*2/*m*) high-temperature modification of K-feldspar, has been examined at 23° C with neutron diffraction (Brown *et al.*, 1974) and at 23°, 400° and 800° C with X-ray diffraction (Ribbe, 1963; Weitz, 1972; Phillips and Ribbe, 1973a; Ohashi and Finger, 1974, 1975; Dal Negro *et al.*, 1978). These studies have shown that sanidine may have varying degrees of Si,Al disorder consistent with the monoclinic symmetry (monoclinic Si,Al topochemistries) and have elucidated the nature of the irregular coordination of the alkali cation. Similarly, studies of disordered Na feldspars (Ribbe *et al.*, 1969; Wainwright, unpublished, see Smith, 1974; Prewitt *et al.*, 1976; Winter and Ghose, 1977; Winter *et al.*, 1979), which are all triclinic (*C*1) at room temperature, have shown that they only become monoclinic (monalbite, *C*2/*m*) upon rapid heating through a displacive transformation when the Na-feldspar is very highly to fully disordered and has monoclinic Si,Al topochemistry. Disordered Na-feldspar with triclinic Si,Al topochemistry is termed high albite whereas Na-feldspar that has monoclinic Si,Al topochemistry but a triclinic morphology (*i.e.*, at temperatures below the displacive transformation) is termed analbite. These studies have also indicated the possibility of positional disorder of the alkali cation (M) site in the collapsed and elongated cavity at room temperature and have characterized the nature of the expansion or inflation of the M-site cavity upon rapid heating.

Less is known about the structures of disordered alkali feldspars with intermediate composition. Anorthoclases, one of the most abundant naturally-occurring alkali feldspars of this type, are recog-

0003–004X/82/0910–0975$02.00

nized by petrographers by their volcanic association, rhombic shape and fine polysynthetic, often cross-hatched ("tartan") twinning. In terms of Si,Al order they may occur as topochemically triclinic K,Ca–high albite, topochemically monoclinic K,Ca–analbite or a cryptoperthitic intergrowth of Na–sanidine and K,Ca–analbite or K,Ca–high albite. Though there are some problems with compositional criteria (De Pieri *et al.*, 1977), the compositional limits of anorthoclases are as indicated in Figure 1 (adapted from Kroll and Bambauer, 1981). Included are cryptoperthites in which the heated phase assemblages consist of monoclinic feldspars or a single homogenized monoclinic feldspar. Only one published refinement of an anorthoclase is available (De Pieri and Quareni, 1973), but as it was refined from film data, the precision is not comparable to that of other refinements on disordered alkali feldspars. Thus we do not have the information about disordered Na-rich alkali feldspar structures needed to make comparisons with the near end-member composition structures, or to allow the desirable thermodynamic calculations of their equations of state (*cf.* Thompson *et al.*, 1974).

A structural study has been completed on three natural low-Ca (less than An_{10}) anorthoclase (K–analbite) samples at room temperature and at temperatures at which the crystals are monoclinic (from 400° to 750° C. The results of this study are reported in two parts. This first part treats the features of the crystal structure and cell geometry related to variations in alkali chemistry and temperature. The second part deals with Si,Al order and the specific nature of apparent thermal motion.

Materials and methods

Specimens of anorthoclase were provided by W. S. MacKenzie and the National Museum of Natural History of the Smithsonian Institution. Specimens from three localities were selected: Grande Caldeira, Azores, $Or_{32.5}Ab_{66.7}An_{0.8}$ (fragments from lavas, #15 of Carmichael and MacKenzie, 1964); Mt. Gibele, Pantelleria Islands, Italy, $Or_{22.3}Ab_{70.8}An_{6.9}$ (loose phenocrysts, #12 of Carmichael and MacKenzie, 1964); and Kakanui, New Zealand, $Or_{13.8}Ab_{83.7}An_{2.5}$ (as xenocrysts in Deborah volcanic sequence, NMNH #133868, see Dickey, 1968). The most K-rich anorthoclase was a cryptoperthite

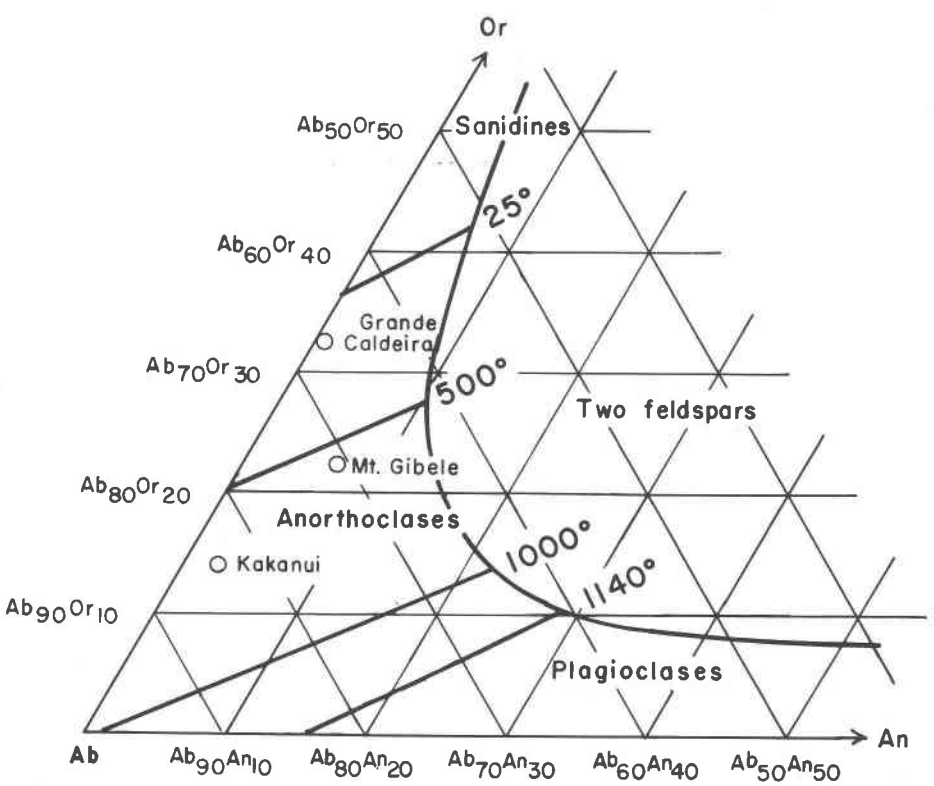

Fig. 1. The phase diagram in the Na–feldspar corner of the feldspar composition triangle: solid lines with temperatures (°C) indicate the approximate point at which K,Ca–analbites become monoclinic (after Fig. 8, Kroll and Bambauer, 1981). Samples examined in this study are shown by circles. Compositions are in mole percent.

consisting of a monoclinic K-rich phase (Na–sanidine) and a twinned triclinic Na-rich phase (K–analbite). Fragments of the cryptoperthitic material were placed in a platinum capsule and heated in an electric furnace at 700° C, within the stability field of single alkali feldspar (*cf.* Luth *et al.*, 1974), for approximately 24 hours to homogenize the sample. Subsequent X-ray reexamination confirmed the homogenization, and suitable crystals were then selected for structure analysis.

The samples selected for intensity data collection were cleavage fragments, generally bounded by (001), (010), and ($\bar{2}$01) or (100). Approximate dimensions of the fragments used are given in Table 1. The chemical composition of the specimens (Table 2) was determined with an ARL-EMX electron microprobe using the data reduction method of Bence and Albee (1968) with the factors of Albee and Ray (1970). No inhomogeneities or Sr or Ba were detected in the samples.

The furnaces used for the high-temperature X-ray examination (one for the precession camera and one for the diffractometer) are a modification of the design of Brown *et al.* (1973) that allow for easier furnace alignment. For a complete description see Harlow (1977).

Table 2. Electron microprobe analyses

Wt. %	Grande Caldeira	Mt. Gibele	Kakanui	
CaO	0.17	1.5	0.53	0.79
K_2O	5.9	3.9	2.5	2.05
Na_2O	7.9	8.2	9.9	9.44
TiO_2	-	0.09	-	-
Fe_2O_3	0.43	-	0.17	minor
SiO_2	66.6	65.7	65.4	67.4
Al_2O_3	18.6	19.5	20.4	20.1
Total	99.6	98.8	98.9	99.88†
Cations per 8 oxygen atoms				
Ca	0.008	0.069	0.026	0.04
K	0.334	0.224	0.141	0.12
Na	0.686	0.710	0.856	0.81
Subtotal	1.028	1.003	1.023	0.97
Ti	-	0.003	-	-
Fe	0.014	-	0.006	-
Si	2.994	2.952	2.927	2.97
Al	0.987	1.036	1.077	1.05
Total	5.023	4.994	5.033	4.99
Feldspar component (mol.%)				
Or	32.5	22.3	13.8	12.1
Ab	66.7	70.8	83.7	84.0
An	0.8	6.9	2.5	3.9
Si:R*	3.02	3.05	2.77	2.94
R_2O_3	1.01	1.07	1.02	1.04

† Dickey (1968)
* R is the total of Fe^{+3} and Al^{+3}; R_2O_3 is normalized to the anorthite content to examine possible non-stoichiometry of the feldspar

Table 1. Structure refinement information and sample sizes

	Grande Caldeira	Mt. Gibele	Kakanui
Room Temperature:			
Reflections collected	2026	1846	3002
Initial unrejected	2003	1822	2460
Final unrejected	1834	1697	2141
Rw isotropic	0.061	0.090	0.107
Ru isotropic	0.080	0.097	0.118
Rw anisotropic	0.035	0.041	0.052
Ru anisotropic	0.046	0.047	0.058
High Temperature ($C\bar{1}$):	400°	510°	750°
Reflections collected	2030	1403	2039
Initial unrejected	2016	*	2002
Final unrejected	1671		1752
Rw isotropic	0.111		0.096
Ru isotropic	0.138		0.119
Rw anisotropic	0.062		0.063
Ru anisotropic	0.074		0.074
High Temperature (C2/m):	400°	510°	750°
Initial unrejected	1050	1044	1043
Final unrejected	855	931	899
Rw isotropic	0.077	0.062	0.067
Ru isotropic	0.127	0.089	0.085
Rw anisotropic	0.043	0.043	0.022
Ru anisotropic	0.073	0.047	0.105
Crystal dimensions in microns	150x 70x 50	190x 140x 90	160x 90x 80

* full triclinic data set not collected

Crystals selected for high-temperature study were cemented to silica–glass fibers. Encapsulation in silica–glass capillaries was not deemed necessary because there was no iron in the samples to cause oxidation problems, and because the highest temperatures were to be below 800° C, judged low enough not to cause alkali sublimation. For temperatures below 400° C, Dupont NR-150B2 polyimide binder solution (supplied courtesy E. I. Dupont de Nemours & Co.) was used. For temperatures of 400° C or greater, the clear cement in Ceramabond 503 High-Temperature Adhesive (Aremco Products, Inc.) was used. No diffraction contribution from the cements was noticed.

The temperature of the displacive monoclinic/triclinic inversion for the feldspars was estimated by examining X-ray precession photographs taken at temperatures up to about 50° above the estimated inversion. Precession photographs confirmed that the crystals had attained monoclinic symmetry. Later the twin angle on a-axis nets $2\cdot(90 - \alpha^*)$ was measured at several elevated temperatures, and inversion temperatures were estimated by plotting

$\cos^2\alpha^*$ *vs.* temperature (see Fig. 2) as suggested by Thompson *et al.* (1974). All three crystals selected for high-temperature structure refinement appeared to be monoclinic at elevated temperatures, however, the most K-rich, Grande Caldeira, showed some streaking of diffraction spots in the directions of the old twin displacements at temperatures 100° above that of the estimated transition. This streaking indicates that some residual strain or dislocations in the crystal existed and prevented all parts from attaining monoclinic symmetry. However, this effect was minor and not considered so serious as to preclude structure analysis.

Intensity data were collected on an automated Picker FACS-1 single-crystal diffractometer using unfiltered MoKα radiation at a 3° take-off angle. Orientation of a crystal for data collection was provided by a least-squares refinement of 12 manually centered reflections, which also yielded initial unit cell parameters. Data were collected in one half of the limiting sphere of reciprocal space from 5° to 60° or 70° two theta ($0.062 \leq \sin\theta/\lambda \leq 0.705$ or 0.809) using the θ–2θ scan technique with a scan speed of 1°/min and an approximate 2.4° scan range (extended for $K\alpha_1$–$K\alpha_2$ dispersion). Background counts were measured for 20 seconds on each side of the peak. Two standard reflections were collected every 49 reflections. The total number of collected intensities and initially unrejected ones are listed in Table 2. Initial rejection of structure data was based on evidence of interference due to overlap from $K\beta$ X-radiation or from the other twinned portion of a crystal. For the Kakanui crystal, which was intimately twinned with nearly equal volumes in the two orientations, a larger number of reflections were lost due to overlap. Therefore more reflections were collected (the half-sphere up to 70° 2θ), and a computer program was developed to determine which reflections might need to be rejected (see Harlow, 1977, for details).

A full triclinic data set was collected at high temperature for the following reasons: first, to compare the intensity of the reflections that are equivalent by monoclinic symmetry (*hkl versus* $h\bar{k}l$); second, to be able to refine a triclinic structure and compare it with the requirements of monoclinic symmetry, and third, to gain an increased accuracy by averaging the equivalent reflections before refinement of the monoclinic structure. The temperature of the diffractometer furnace was set at a value approximately 50° C above the measured inversion temperature. Scans of the 005 reflection in the b^*–c^* plane (normally by means of a chi rotation) and the 12 reflections used for orientation through θ–2θ were made to check for splitting. These two steps were repeated until no peak splitting was found and to be sure that the crystals were no longer twinned, *i.e.*, were monoclinic. After refining the orientation matrix obtained from the 12 reflections, the cell parameters were checked to insure that they were monoclinic within the error of measurement.

After intensity data were collected, the positions of approximately 40 to 50 reflections ($\sin\theta/\lambda \geq 0.34$) were measured and the values were entered in a modified version of Burnham's (1962) LCLSQ (lattice cell least squares) refinement program. The results are given in Table 3.

The crystals were reexamined with the precession technique after data collection at high temperatures was completed. In all three cases the number of twin-related orientations and the relative proportions of twin orientations that had originally existed changed significantly. The change was most marked for the Grande Caldeira crystal, which shows beautiful M-type twinning that according to Laves (1950) can only be caused by a transformation from monoclinic to triclinic symmetry. Because the highest temperature that any crystal experienced between the two precession examinations was that at which the intensity data were collected, the crystals must have been monoclinic during data collection. The intensity data were corrected for background, scaled to a uniform level relative to standard reflec-

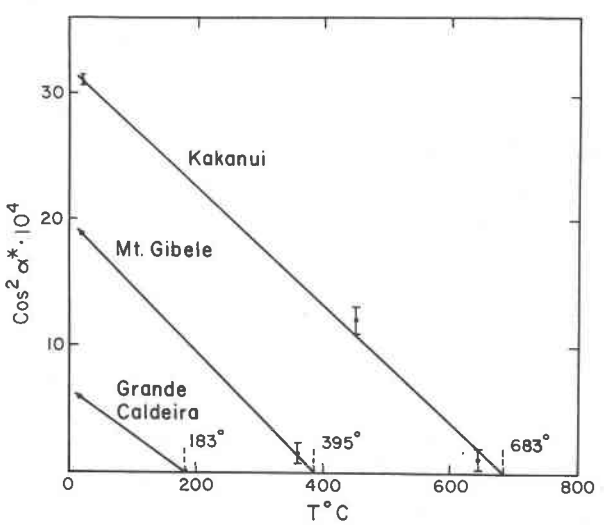

Fig. 2. Plot of $\cos^2\alpha^*$ for each anorthoclase (K–analbite) against temperature. Lines are fit by least squares; inversion temperatures (intercept) are shown.

Table 3. Cell parameters

T (°C)	a (Å)	b (Å)	c (Å)	α (°)	β (°)	γ (°)	V (Å^3)	α* (°)	γ* (°)
Grande Caldeira Or 32.5									
23° C$\bar{1}$	8.290(2)	12.966(3)	7.151(2)	91.18(2)	116.31(1)	90.14(2)	688.8(3)	88.62(2)	89.26(2)
183° C$\bar{1}$	8.3108(8)	12.9729(9)	7.1578(6)	90.007(5)	116.187(5)	90.033(6)	692.5(1)	89.976(5)	89.960(6)
400° C2/m	8.3482(7)	12.9800(7)	7.1582(5)	90.0	116.109(5)	90.0	696.5(1)	90.0	90.0
Mt. Gibele Or 22.3									
23° C$\bar{1}$	8.252(2)	12.936(2)	7.139(1)	92.11(1)	116.32(1)	90.22(1)	682.4(2)	87.54(1)	88.71(1)
388° C$\bar{1}$	8.290(4)	12.954(30	7.150(3)	90.75(2)	116.18(2)	90.35(2)	689.1(6)	89.34(2)	89.98(2)
510° C2/m	8.314(1)	12.973(2)	7.150(1)	90.0	116.135(8)	90.0	692.4(2)	90.0	90.0
Kakanui Or 13.8									
23° C$\bar{1}$	8.2168(6)	12.9166(7)	7.1270(5)	92.754(4)	116.357(4)	90.239(5)	676.7(1)	86.808(4)	88.367(5)
700° C2/m	8.311(1)	12.972(2)	7.148(1)	90.0	116.071(7)	90.0	692.2(2)	90.0	90.0
750° C2/m	8.321(2)	12.969(2)	7.148(1)	90.0	116.05(1)	90.0	693.0(3)	90.0	90.0

Estimated standard deviations in parentheses refer to the last digits

tion intensities, and corrected for Lorentz-polarization effects. No absorption or extinction corrections were applied as all crystals had maximum dimensions less than 0.2 mm and linear absorption coefficients (μ) less than 11 cm^{-1}.

The structure factors were entered in L. W. Finger's RFINE II (Geophysical Laboratory) full-matrix least-squares refinement program. Relativistic Dirac-Slater X-ray scattering factors (Cromer and Waber, 1965) for neutral atoms were employed. Occupancies of Na, K, and Ca in the alkali cation (M) site were based on atomic proportions. Tetrahedrally coordinated cation (T) sites were assumed to be completely disordered so that the Al and Si occupancies in each T site were evaluated as $(1 + X_{an})/4$ and $(3 - X_{an})/4$, respectively (where X_{an} is the mole fraction of $CaAl_2Si_2O_8$ in the crystal). Each observed structure factor was weighted for refinement as $1/\sigma$ where σ is the standard deviation of F_{obs} based on counting statistics. For the monoclinic refinements the average of F_{obs} was set as the larger of two estimates of the variance of the sampling, one calculated including counting statistics and the other calculated strictly from the sampling. Reflections for which F_{obs} was zero or less than three sigma of the background intensity were treated as unobserved.

The triclinic least-squares refinements were carried out in the normal fashion starting with values from the refinement of a high albite by Wainwright (unpublished, see Smith, p. 86, 1974); resulting R factors are listed in Table 1. The results from the final anisotropic refinements were used in most evaluations of structural parameters and are listed in Table 4. A large anisotropy for the M-site temperature factor was expected (*e.g.*, Ribbe *et al.*, 1969), but in fact all room-temperature refinements produced M-sites with non-positive-definite ellipsoids (one ellipsoid displacement was imaginary) of apparent vibration. Consequently, and to be consistent with refinements of high albite and monalbite (Ribbe *et al.*, 1969; Prewitt *et al.*, 1976; Winter *et al.*, 1979), the M-site was refined with various models using partial atoms on multiple sites. These partial-atom sites will be called subsites and denoted by subscript notation, *e.g.*, M_1 and M_2. All such refinements use isotropic partial atoms except the "split-species" models (see discussion) because anisotropic treatments of the subsites usually develop very large correlations among the supposedly independent parameters and will not converge in refinement. For the latter configuration, the sequence of refinement steps was to increase the number of independent parameters, refining first the positions of the subsites, holding isotropic temperature factors (B) constant, then a common B, then independent B's, and finally the constrained occupancies of the subsites (the amount of the average M-site atom on each site). These steps in the refinement of a model with a given number of subsites were followed until that model would not converge in the least-squares treatment. The number of subsites was sequentially increased from two to three to four, *etc.*, for each structure, until an

Table 4. Positional and thermal parameters

	X	Y	Z	β_{11}	β_{22}	β_{33}	β_{12}	β_{13}	β_{23}
				$\beta \times 10^4$					
Grande Caldeira 23°									
T_1O	0.0085(1)	0.1753(1)	0.2207(1)	56(2)	17(1)	51(2)	-4(1)	28(1)	0(1)
T_1m	0.0069(1)	0.8180(1)	0.2252(1)	53(2)	15(1)	51(2)	7(1)	26(1)	2(1)
T_2O	0.6954(1)	0.1140(1)	0.3354(1)	51(2)	11(1)	65(2)	0(1)	26(1)	2(1)
T_2m	0.6941(1)	0.8815(1)	0.3465(1)	54(2)	11(1)	63(2)	3(1)	27(1)	1(1)
M	0.2750(2)	0.0013(1)	0.1366(2)	-14(2)	65(1)	139(5)	2(1)	-7(3)	-52(2)
O_{A1}	0.0016(3)	0.1388(2)	0.9947(3)	124(5)	30(2)	97(6)	6(2)	61(5)	4(2)
O_{A2}	0.6056(3)	0.9972(2)	0.2828(4)	86(5)	18(1)	124(6)	1(2)	32(4)	2(2)
O_BO	0.8233(3)	0.1279(2)	0.2180(4)	95(5)	41(2)	158(7)	-10(2)	75(5)	5(3)
O_Bm	0.8227(3)	0.8574(2)	0.2329(4)	94(5)	39(2)	151(7)	11(2)	71(5)	-2(3)
O_CO	0.0233(3)	0.3012(2)	0.2618(4)	88(4)	22(1)	122(6)	-3(2)	44(4)	-3(2)
O_Cm	0.0241(3)	0.6916(2)	0.2421(4)	84(4)	20(1)	118(6)	3(2)	30(4)	4(2)
O_DO	0.1897(3)	0.1204(2)	0.4004(3)	90(5)	25(1)	87(6)	6(2)	23(4)	8(2)
O_Dm	0.1883(3)	0.8725(2)	0.4125(4)	86(5)	27(1)	95(5)	-3(2)	22(4)	-7(2)
Grande Caldeira 400°									
T_1	0.0091(2)	0.1797(1)	0.2238(3)	135(3)	31(1)	106(3)	-8(2)	76(3)	-2(2)
T_2	0.6985(2)	0.1167(1)	0.3431(2)	132(3)	25(1)	124(4)	-2(2)	75(3)	-1(2)
M	0.2796(5)	0.0	0.1366(7)	95(8)	107(4)	334(17)	0	87(9)	0
O_{A1}	0.0	0.1408(6)	0.0	240(12)	49(4)	98(11)	0	96(9)	0
O_{A2}	0.6157(9)	0.0	0.2884(12)	190(14)	32(3)	194(20)	0	89(14)	0
O_B	0.8242(5)	0.1373(4)	0.2236(7)	182(8)	64(3)	290(14)	-6(7)	159(9)	11(9)
O_C	0.0275(6)	0.3078(3)	0.2544(9)	187(10)	37(3)	280(16)	-12(6)	136(11)	-14(7)
O_D	0.1883(5)	0.1248(4)	0.4087(6)	190(9)	45(3)	209(12)	15(6)	82(8)	16(7)
Mt. Gibele 23°									
T_1O	0.0085(1)	0.1711(1)	0.2185(2)	85(2)	19(1)	69(2)	0(1)	47(2)	5(1)
T_1m	0.0060(1)	0.8164(1)	0.2271(2)	82(2)	16(1)	66(2)	11(1)	44(2)	8(1)
T_2O	0.6933(1)	0.1115(1)	0.3289(2)	80(2)	13(1)	84(2)	5(1)	44(2)	5(1)
T_2m	0.6904(1)	0.8798(1)	0.3496(1)	84(2)	13(1)	81(2)	7(1)	45(2)	6(1)
M	0.2743(2)	0.0033(2)	0.1353(3)	0(3)	74(2)	167(6)	7(2)	-3(3)	-91(2)
O_{A1}	0.0033(4)	0.1377(2)	0.9907(4)	150(6)	35(2)	109(7)	12(3)	76(6)	12(3)
O_{A2}	0.5994(4)	0.9945(2)	0.2802(4)	117(6)	19(1)	138(7)	5(2)	52(5)	8(3)
O_BO	0.8219(4)	0.1194(2)	0.2092(4)	128(6)	44(2)	177(8)	1(3)	96(6)	11(3)
O_Bm	0.8212(4)	0.8531(2)	0.2381(4)	117(6)	44(2)	171(8)	14(3)	87(6)	4(3)
O_CO	0.0207(4)	0.2964(2)	0.2688(4)	115(6)	27(2)	137(7)	1(2)	63(5)	-1(3)
O_Cm	0.0227(4)	0.6899(2)	0.2312(4)	116(6)	24(2)	128(7)	9(2)	44(5)	6(3)
O_DO	0.1916(4)	0.1171(2)	0.3943(4)	126(6)	29(2)	105(7)	9(2)	44(5)	11(3)
O_Dm	0.1881(4)	0.8701(2)	0.4191(4)	116(6)	29(2)	115(7)	5(2)	38(5)	1(3)
Mt. Gibele 510°									
T_1	0.0081(1)	0.1792(1)	0.2236(2)	93(2)	28(1)	92(2)	-9(1)	49(2)	-2(1)
T_2	0.6967(1)	0.1164(1)	0.3422(2)	87(2)	21(1)	111(2)	-3(2)	47(2)	-2(1)
M	0.2780(3)	0.0	0.1372(4)	60(5)	106(3)	291(9)	0	48(6)	0
O_{A1}	0.0	0.1391(3)	0.0	202(9)	56(3)	129(9)	0	96(8)	0
O_{A2}	0.6084(5)	0.0	0.2842(6)	123(8)	28(2)	219(11)	0	51(8)	0
O_B	0.8230(4)	0.1361(2)	0.2242(5)	145(6)	70(2)	282(9)	-25(3)	139(6)	-6(4)
O_C	0.0256(4)	0.3044(2)	0.2528(5)	148(6)	35(2)	250(8)	-15(3)	86(6)	-7(3)
O_D	0.1877(4)	0.1241(2)	0.4063(4)	153(6)	56(2)	153(7)	10(3)	35(5)	19(3)
Kakanui 23°									
T_1O	0.0087(1)	0.1686(1)	0.2168(1)	47(1)	19(1)	73(2)	-5(1)	29(1)	-4(1)
T_1m	0.0054(1)	0.8153(1)	0.2275(1)	44(1)	18(1)	68(2)	3(1)	27(1)	-2(1)
T_2O	0.6923(1)	0.1099(1)	0.3256(1)	44(1)	14(1)	82(2)	-2(1)	25(1)	-2(1)
T_2m	0.6886(1)	0.8789(1)	0.3514(1)	45(1)	15(1)	83(2)	0(1)	28(1)	-2(1)
M	0.2743(2)	0.0051(2)	0.1350(3)	-16(3)	115(3)	227(6)	5(2)	-21(3)	-144(3)
O_{A1}	0.0045(4)	0.1369(2)	0.9881(4)	113(5)	33(2)	117(6)	0(2)	63(5)	-3(2)
O_{A2}	0.5969(3)	0.9925(2)	0.2818(4)	75(4)	23(2)	118(6)	-3(2)	34(4)	4(2)
O_BO	0.8220(4)	0.1145(2)	0.2051(4)	90(5)	36(2)	164(7)	-10(2)	74(5)	-4(3)
O_Bm	0.8203(4)	0.8499(3)	0.2422(4)	81(5)	45(2)	169(7)	6(2)	72(5)	-10(3)
O_CO	0.0188(3)	0.2940(2)	0.2724(4)	77(4)	24(2)	158(7)	-6(2)	50(4)	-9(2)
O_Cm	0.0225(3)	0.6882(2)	0.2267(4)	77(4)	27(2)	107(6)	6(2)	21(4)	3(2)
O_DO	0.1932(3)	0.1146(2)	0.3911(4)	80(4)	29(2)	102(6)	4(2)	20(4)	4(2)
O_Dm	0.1882(4)	0.8685(2)	0.4232(4)	76(4)	34(2)	109(6)	-4(2)	11(4)	15(2)
Kakanui 750°									
T_1	0.0089(3)	0.1796(2)	0.2240(3)	144(3)	54(1)	163(4)	-11(2)	88(2)	-2(2)
T_2	0.6972(2)	0.1170(2)	0.3437(2)	121(2)	45(1)	202(4)	-3(2)	81(2)	-1(1)
M	0.2839(7)	0.0	0.1496(10)	126(8)	247(12)	619(28)	0	70(13)	0
O_{A1}	0.0	0.1378(8)	0.0	327(11)	83(7)	263(13)	0	151(10)	0
O_{A2}	0.6115(9)	0.0	0.2858(16)	145(16)	55(5)	508(34)	0	14(18)	0
O_B	0.8282(5)	0.1382(7)	0.2288(7)	211(9)	123(7)	407(16)	-31(9)	202(10)	18(13)
O_C	0.0320(5)	0.3030(5)	0.2563(9)	251(11)	64(4)	397(18)	-30(7)	150(11)	-6(9)
O_D	0.1850(5)	0.1251(6)	0.4121(5)	266(12)	84(5)	267(14)	23(8)	106(8)	19(10)

Estimated standard deviations in parentheses refer to last digits

improvement was seen over the anisotropic model or until the subsite model failed to converge. The results for these final steps in M-site model refinements are listed in Table 5.

Essentially the same three steps were followed for the three high-temperature structure refinements except that initially the triclinic F_{obs} data sets were refined in space group C1 to test the consistency of the data with monoclinic symmetry. The starting parameters were those of the room-temperature refinements for the same crystal and the resulting triclinic structures were consistent with monoclinic symmetry within the estimated errors of all refined parameters except for anisotropic thermal parameters. Thus the data were averaged into a monoclinic set. No attempt was made in any of the least-squares procedures to refine on the Si,Al occupancy of the T sites. At various stages of the refinement of the M-site models, difference Fourier sections were made of the M-site region parallel to the *b–c* plane to evaluate the quality of the fit.

Interatomic distances and angles and root-mean-square displacements for thermal-ellipsoidal axes were calculated in the RFINE II program. Estimated errors for these structural parameters were calculated with Finger's ERROR.

Table 5. Ellipsoids of thermal expansion strain

Case	†	Unit Strain (/°C or /Or%)	Angle to +a	+b	+c
1)	1	8.5(1) E-5	81.2(3)	48.4(6)	55.0(5)
Grande	2	1.4(2) E-5	8.9(8)	96.9(9)	121.6(5)
Caldeira	3	-6.6(1) E-5	88.8(7)	42.5(5)	129.1(4)
23°-183°	V	3.4(3) E-5			
2)	1	2.4(1) E-5	22(2)	86(1)	95(2)
Grande	2	2.5(6) E-6	98(2)	11(6)	80(60
Caldeira	3	0.0(6) E-6	110(2)	100(6)	11(6)
183°-400°	V	2.7(1) E-5			
3)	1	6.7(1) E-5	82(1)	47.6(7)	55.8(6)
Mt. Gibele	2	1.2(2) E-5	8(1)	96(1)	121.8(3)
23°-388°	3	-5.2(1) E-5	90.1(7)	42.9(6)	129.6(5)
	V	2.7(4) E-5			
4)	1	2.6(8) E-5	27(6)	90	89(6)
Mt. Gibele	2	9.7(3) E-6	90	0	90
388°-510°	3	-0.3(5) E-5	116(6)	90	1(6)
	V	3.9(1) E-5			
5)	1	5.16(3) E-5	78.6(4)	48.1(2)	57.8(2)
Kakanui	2	1.50(3) E-5	11.7(4)	99.8(3)	121.9(2)
23°- 700°	3	-3.30(2) E-5	87.3(1)	42.6(1)	131.4(1)
	V	3.36(5) E-5			
6)	1	3.0(6) E-5	22(2)	90	95(2)
Kakanui	2	-0.0(4) E-5	112(2)	90	5(2)
700°-750°	3	-0.4(3) E-5	90	0	90
	V	2.5(8) E-5			
7)	1	1.0(3) E-4	79(2)	49(1)	58(1)
Kakanui -	2	4.9(3) E-4	12(2)	100(2)	121(2)
Mt. Gibele	3	-5.2(2) E-4	86.6(4)	42.7(6)	131.8(5)
23°	V	9.8(5) E-4			
8)	1	11.8(2) E-4	82.0(9)	46.4(8)	56.8(6)
Mt. Gibele -	2	4.3(3) E-4	8(1)	96(1)	121.2(5)
Grande	3	-6.9(2) E-4	89.5(8)	44.3(7)	131.1(5)
Caldeira	V	9.2(5) E-4			
23°					
9)	1	7.4(9) E-4	22(3)	90	93(3)
Mt. Gibele	2	1.7(4) E-4	90	0	90
388° -	3	1.4(7) E-4	112(3)	90	5(3)
Grande	V	1.1(1) E-3			
Caldeira 400°					

* E-n + x 10^{-n}

† 1, 2, 3 are the maximum, intermediate, and minimum ellipsoid axes and V is the volumetric component
Estimated standard deviations in parenthesis refer to last digits

Results and discussion

Lattice parameters

Cell parameters for the three anorthoclase specimens at 23° C and at elevated temperatures are listed in Table 3 and are plotted in Figures 3 and 4. The room-temperature cell dimensions are consistent with alkali feldspars having nearly complere Si,Al disorder. The values lie close to lines connecting analbite and high sanidine on the α^*–γ^* and *b–c* plots. The α^*–γ^* relations indicate the difference in Al content of the T_1 sites ($t_1$0–t_1m; Al in $T_1$0 minus Al in T_1m), which is a measure of topochemical triclinicity, whereas the *b–c* plot indicates the total Al content in the T_1 sites (either $t_1$0 + t_1m for triclinic structures or t_1 for monoclinic ones). MacKenzie and Smith (1962) found that in ordered albitic plagioclases an increase in An content causes an effect similar to an increase in disorder. On the basis of the limited work on ternary feldspars like anorthoclases (Hakli, 1960; Carmichael and MacKenzie, 1964; Boudette and Ford, 1966; Kroll and Bambauer, 1981), the use of cell-parameter plots for evaluating Si,Al order appears valid for the samples under investigation. It is natural to expect the values of $t_1$0–t_1m to approach zero as these feldspars become optically (Grande Caldeira and Mt. Gibele by Carmichael and MacKenzie, 1964) and dimensionally monoclinic at elevated temperatures. The results from the least-squares cell parameter refinements support the conclusion of monoclinic symmetry and consequent monoclinic Si,Al topochemistry.

It is common for perthitic intergrowths of alkali feldspar containing coherent composites of two phases to have "anomalous" values of *a*, measured in Δa (= $a_{obs} - a_{est}$, see Stewart and Wright, 1974; Stewart, 1975). None of the anorthoclases examined in this study show Δa values greater than

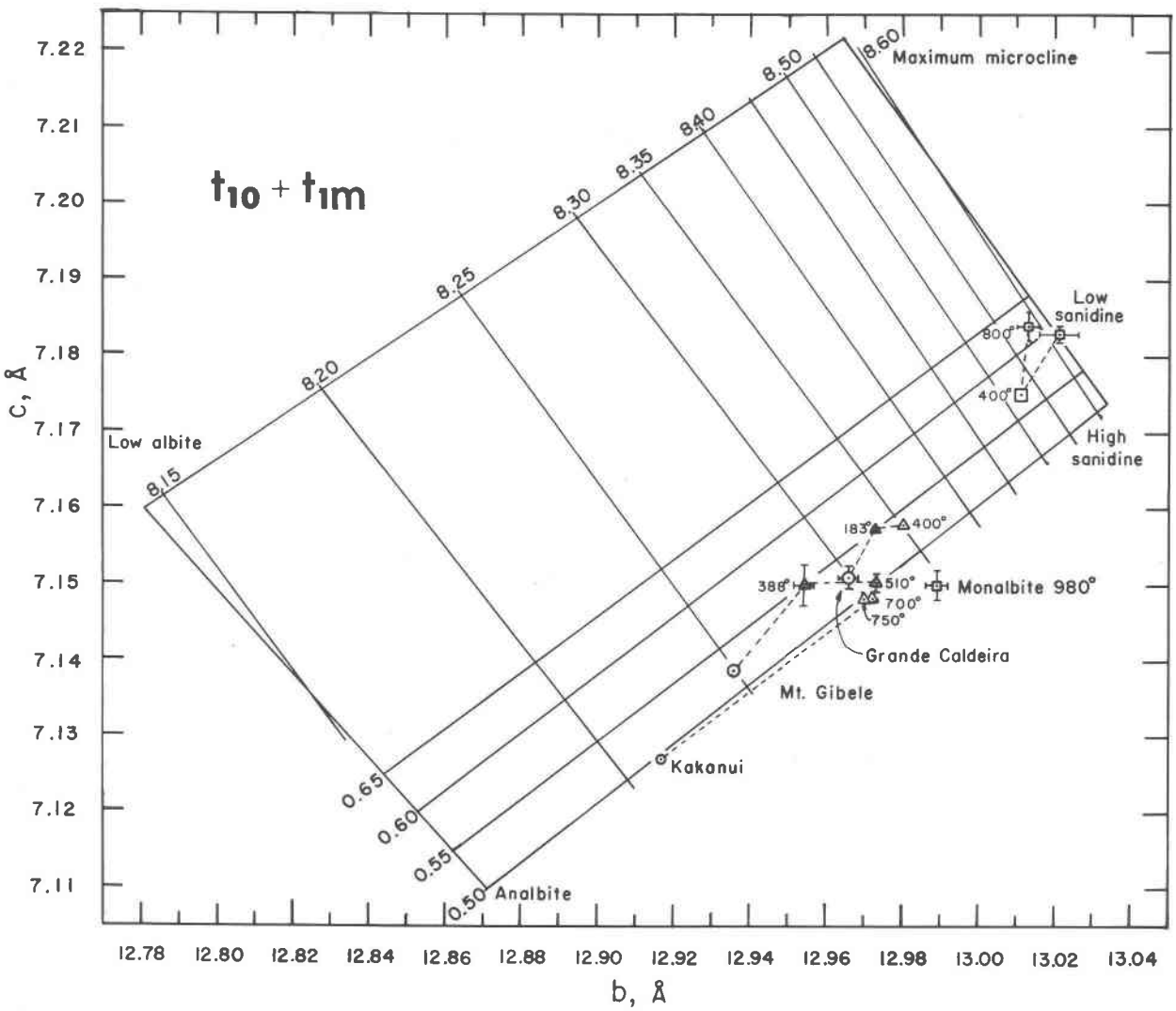

Fig. 3. The *b–c* plot, after Stewart and Wright (1974), for room- and high-temperature data (see text); contours from 8.15 to 8.60 are for the *a* cell edge; contours from 0.50 to 0.65 are for $t_1 0 + 1_1 m$ (the Al occupancies of the $T_1 0$ and $T_1 m$ sites). Heating produces an effect similar to that of an increase in K-feldspar content—displacement to the upper right, parallel to lines of constant structural state.

0.01Å whereas a minimum value of 0.05 is considered sufficient to indicate strain.

The overall effect of rapid increase in temperature on cell dimension (within the limits of the experiment, *i.e.*, $T < 800°$) appears to be the same as an increase in Or content of a feldspar assuming Si,Al order is constant. This result is consistent with the results of Grundy and Brown (1969) and Kroll *et al.* (1980).

An estimate of the composition for the displacive triclinic/monoclinic inversion (Or disp) at room temperature has been made by plotting $\cos^2\alpha$ (at room temperature) *vs.* Or content in Figure 5. A value for an analbite (F9/32 from Grundy and Brown, 1969) is also included. A linear relationship is expected for alkali feldspars having the same degree of monoclinic disorder or the same equilibrium temperature, as shown by Kroll *et al.* (1980). Such an approximation for these three anorthoclases is reasonable based on the *b–c* plot (Fig. 3), and thus a least squares line was fit to the points. The extrapolation of this line to zero predicts a composition of Or_{36} for the displacive inversion at room-temperature. This value compares well with the values of Or_{36} of MacKenzie (1952) and Or_{34-36} of Bambauer *et al.* (1978), Hovis (1980) and Kroll *et al.* (1980).

The relationship between alkali chemistry and

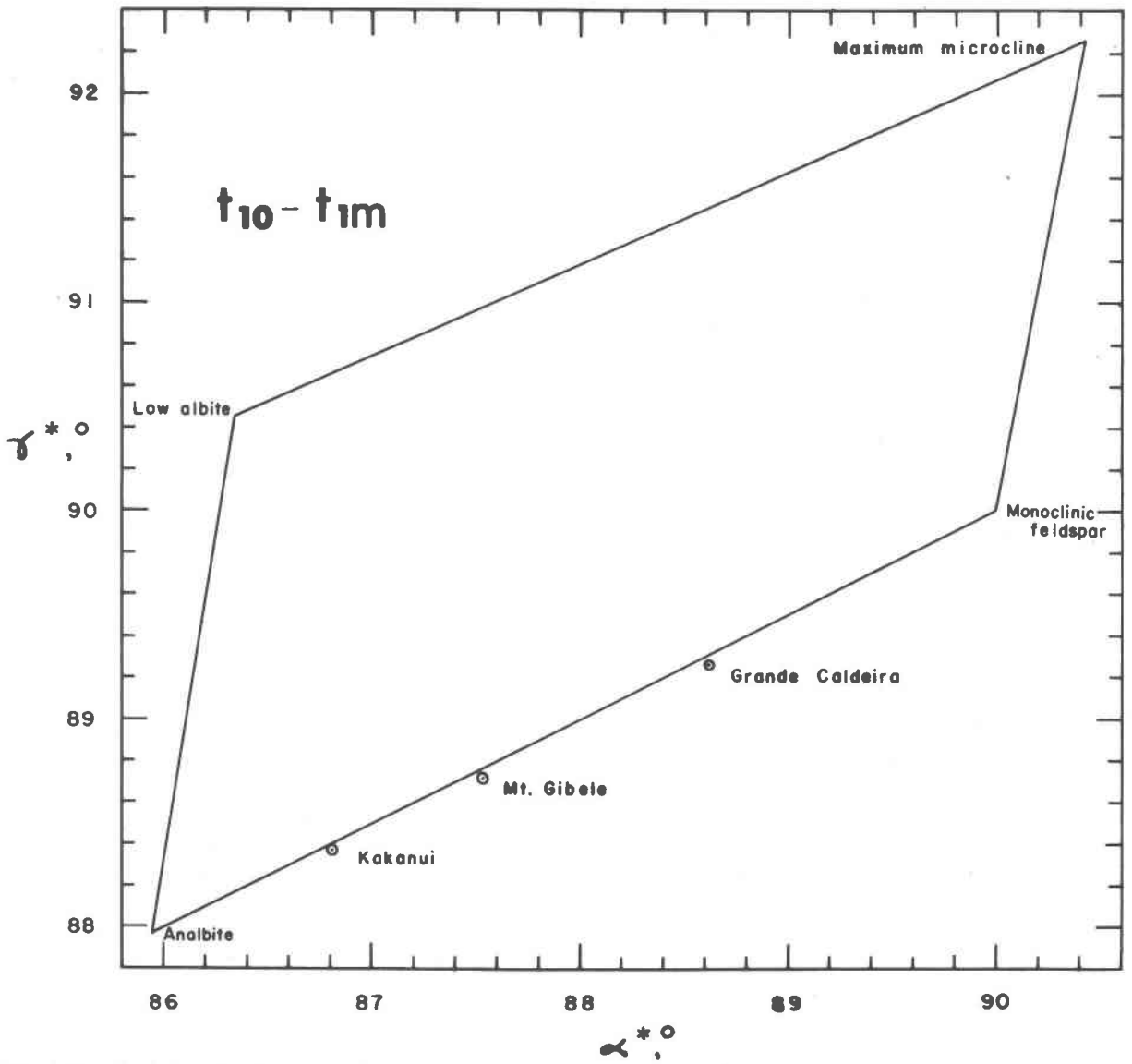

Fig. 4. The α^*–γ^* plot, after Stewart and Wright (1974), used as a measure of triclinic Si,Al order. Room-temperature values for the anorthoclases examined in this study are shown by circles and indicate good agreement with a topochemically monoclinic Si,Al distribution as represented by the line connecting analbite with monoclinic feldspar.

cell parameters at the transition temperature has been estimated by interpolating between the values at higher and lower temperatures in order to evaluate possible limits to the cell parameter values of highly disordered monoclinic alkali feldspars. The linear slopes are nearly flat for transition values, and for a pure K-feldspar estimated values are between 690 and 695Å^3 for the cell volume, 8.30 and 8.35Å for a and 7.15Å for c. The value of b is nearly constant at about 12.97Å with perhaps a slight decrease with increasing Or content. There seem to be unique "transition" values of cell parameters for highly disordered alkali feldspars. Cooling or high pressure experiments would yield actual determination of these limits for more potassic feldspars. The cooling experiment on a high sanidine by Grove and Hazen (1974) has not come close to the transition values. Hazen (1976), on the other hand, did succeed in reaching the inversion at high pressures: 18 kbar for Or_{82} and 12 kbar at Or_{67} with values very close to those indicated by the measurements here. Hence, as suggested by Hazen (1977), there does

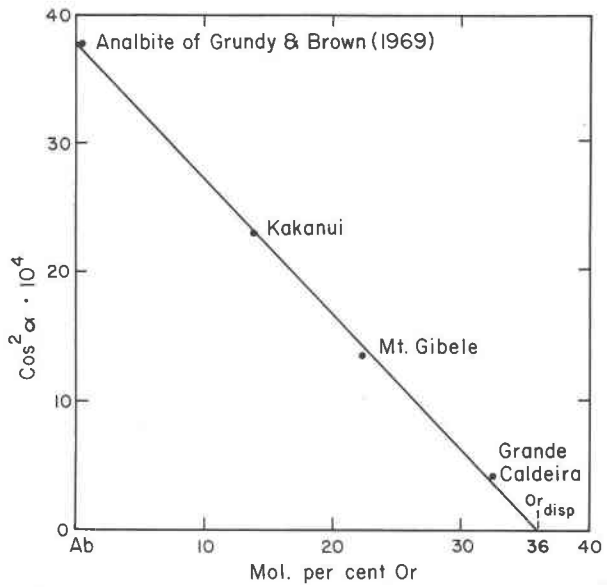

Fig. 5. Plot of $\cos^2\alpha$ at room temperature for the three anorthoclases (K–analbites) and analbite (F9/32, Grundy and Brown, 1969) against Or content. Least squares linear fit indicates a transition composition of Or_{36}.

appear to be a particular structure configuration at the displacive transition which is directly related to unit cell geometry.

The change in cell dimensions upon heating does not necessarily give an adequate picture of the thermal expansion in crystals that have low symmetry because the directions of maximum and minimum expansion or strain are not symmetrically constrained to lie parallel to lattice translations. Ohashi and Burnham (1973) developed a mathematical approach for analyzing small lattice deformations in terms of a second-order thermal strain tensor. A strain analysis was performed on the anorthoclase cell refinements using the program STRAIN, (Ohashi and Finger, 1973) in order to examine the changes with temperature and composition; the results are listed in Table 5. The effects of temperature and of increasing Or content on the orientation of the thermal strain ellipsoid at temperatures below the monoclinic/triclinic transition are almost identical, and are consistent with the results of Ohashi and Finger (1973). Above the transition temperature, the strain ellipsoid must have an axis parallel to the *b* cell edge normal to the (010) mirror plane. The major strain axis rotates slightly, becoming almost parallel to a^*, whereas the other two axes apparently vary with composition; the intermediate and minor axes are reversed between Kakanui and the other two crystals. The results on thermal expansion are virtually identical to those for two synthetic disordered alkali feldspars (Or_{19} and Or_{38}) studied by Henderson (1979). Calculation of the displacements between the Mt. Gibele cell at 388° C and the Grande Caldeira cell at 400° C yield the same result as heating a crystal above the transition temperature, even after taking into account the small difference in temperature.

Crystal structure

Discussion of the anorthoclase (K–analbite) structure in this section is restricted to structural features that show correlations with changes in alkali chemistry and/or temperature. These are M–O bond lengths, T–O–T interatomic angles, and overall and M-cation apparent thermal motion. Hence, some relations which appear to be mainly a consequence of a change from triclinic to monoclinic crystal symmetry are ignored here.

M–O bonding. The alkali cation to oxygen bonding is the structural feature most correlated with triclinicity and the degree of the expansion of the framework structure. In triclinic alkali feldspars coordination about the M site is very irregular, with nine nearest neighbor oxygen atoms within 3.5Å. However, only five to seven of these are within 0.4Å of the shortest M–O distance and can thus be considered the first coordination sphere. Smith (1974) discusses the M-site relations for most feldspars in detail.

In spite of the fact that the average nature of the measured structure obscures the bonding of individual sodium and potassium (and calcium) atoms and that the single atom M-site model is evidently unrealistic (to be treated in a later section), the variation in M–O bond lengths (Table 6 and Figs. 6 and 7) does elucidate several features in the structures. First, as expected, the average M–O distances increase with increasing Or content and with increasing temperature. Second, the variance of the average ⟨M–O⟩ value decreases with increasing Or content and with increasing temperature for any particular composition, indicating the increasing geometric regularity of the cavity for an effectively larger M-site occupant. This increasing regularity is also demonstrated by the decreasing difference in the pseudosymmetrically equivalent bond distance pairs for the room-temperature structures (*i.e.*, ⟨M–$O_{A1}0$⟩ and ⟨M–$O_{A1}c$⟩ or ⟨M–O_B0⟩ and ⟨M–O_Bm⟩). Third, with the exception of ⟨M–O_C⟩, all of the M–O

Table 6. M–O distances for both room- and high-temperature structures including corrections for noncorrelated thermal motion (in Å)

	Grande Caldeira				Mt. Gibele				Kakanui			
	23°		400°		23°		510°		23°		750°	
	raw	noncorr	raw	noncorr	raw	noncorr	raw	noncorr	raw	noncorr	raw	noncorr
M-$O_{A1}0$	2.720(3)	2.742	2.782(3)	2.818	2.684(4)	2.710	2.750(4)	2.786	2.655(4)	2.687	2.775(4)	2.850
-$O_{A1}c$	2.728(3)	2.748			2.722(4)	2.745			2.722(4)	2.752		
-O_{A2}	2.464(3)	2.490	2.524(4)	2.569	2.414(3)	2.446	2.472(4)	2.519	2.389(3)	2.432	2.454(4)	2.564
-O_B0	2.809(3)	2.831	2.934(4)	2.968	2.679(3)	2.709	2.930(4)	2.963	2.611(4)	2.651	2.982(4)	3.043
-O_Bm	3.050(3)	3.063			3.112(4)	3.125			3.159(5)	3.170		
-O_C0	3.203(3)	3.219	3.112(3)	3.145	3.274(4)	3.293	3.140(4)	3.171	3.315(5)	3.336	3.158(5)	3.218
-O_Cm	3.072(3)	3.088			3.015(4)	3.033			2.969(4)	2.991		
-O_D0	2.740(3)	2.761	2.882(4)	2.919	2.642(3)	2.672	2.852(4)	2.884	2.572(4)	2.611	2.912(4)	2.976
-O_Dm	2.930(3)	2.941			3.018(4)	3.029			3.075(4)	3.085		
M-O Av	2.857	2.876	2.882	2.932	2,840	2.863	2.869	2.903	2.830	2.857	2.901	2.971
σ	.228	.224	.180	.150	.276	.270	.207	.202	.311	.300	.217	.202
Length	5.980	6.004	5.816	5.886	6.130	6.154	5.783	5.847	6.235	6.255	5.898	6.019
Width	4.507	4.550	4.574	4.646	4.443	4.494	4.547	4.621	4.408	4.474	4.577	4.745

Length = $\langle M\text{-}O_Bm\rangle + \langle M\text{-}O_Dm\rangle$ Width = $\langle M\text{-}O_{A2}\rangle + \langle M\text{-}O_{A1}\rangle[\cos\frac{1}{2}(O_{A1}\text{-}M\text{-}O_{A1})]$

Estimated standard deviations in parenthese refer to the last digits

bond lengths for high-temperature monoclinic structures increase with respect to monoclinic averages of the room-temperature results for non-corrected distances (Fig. 7). If bond lengths are corrected for apparent thermal motion (both room- and high-temperature structures) this relationship is true for all of the M–O distances. Fourth, the elongate narrow alkali cavity becomes shorter along [0$\bar{1}$1] and wider along [100] with increasing Or content. This feature can be seen for the room-temperature data with the aid of Figure 8. The length of the cavity can be defined by the O_Bm–O_Dm distance or the almost equivalent $\langle M\text{–}O_Bm\rangle$ + $\langle M\text{–}O_Dm\rangle$, both of which decrease with increasing Or content. Similarly, the width of the cavity is related to $\langle M\text{–}O_{A2}\rangle$ + $\langle M\text{–}O_{A1}\rangle$*cos [½($O_{A1}0$–M–$O_{A1}c$)], which increases with increasing Or content. These features can be seen graphically in Figure 8 by following the trends of the M–O values with composition.

The effect of increasing temperature is not simply to inflate the sodium (and calcium) filled cavity isotropically to approach the shape of the cavity when filled with the larger potassium (or rubidium) atom. The inflation is ellipsoidal. Although there is enough increase in effective volume of the alkali cavity to expand the K–analbite structures to monoclinic symmetry at high temperature, each cavity is progressively more elongate (‖ to *b*) and narrow (‖ to [100]) with increasing Na content. The cavities are not a replica of or comparable to that in sanidine. Possible constraints on the inflation geometry, apart from size, may be the charge and mass of the M-site occupant, as these properties influence possible thermal vibration. Results of M-site modeling, described in the following discussion, support this suggestion. A possibly unique feature of the M-site coordination in the high-temperature monoclinic feldspars is the direction of the M-site bonds. Stereographic projections of the M-site coordination for the three crystals are indistinguishable from one another at high temperatures for either the nine immediate oxygens or the twelve closest T sites, but are markedly different at room temperature.

Most of the thermal effect on cell dimensions of these feldspar structures can be explained by shortening of the M–O_Bm, M–O_Dm, and M–O_C0 bonds and lengthening of the M–O_B0, M–O_D0, and M–

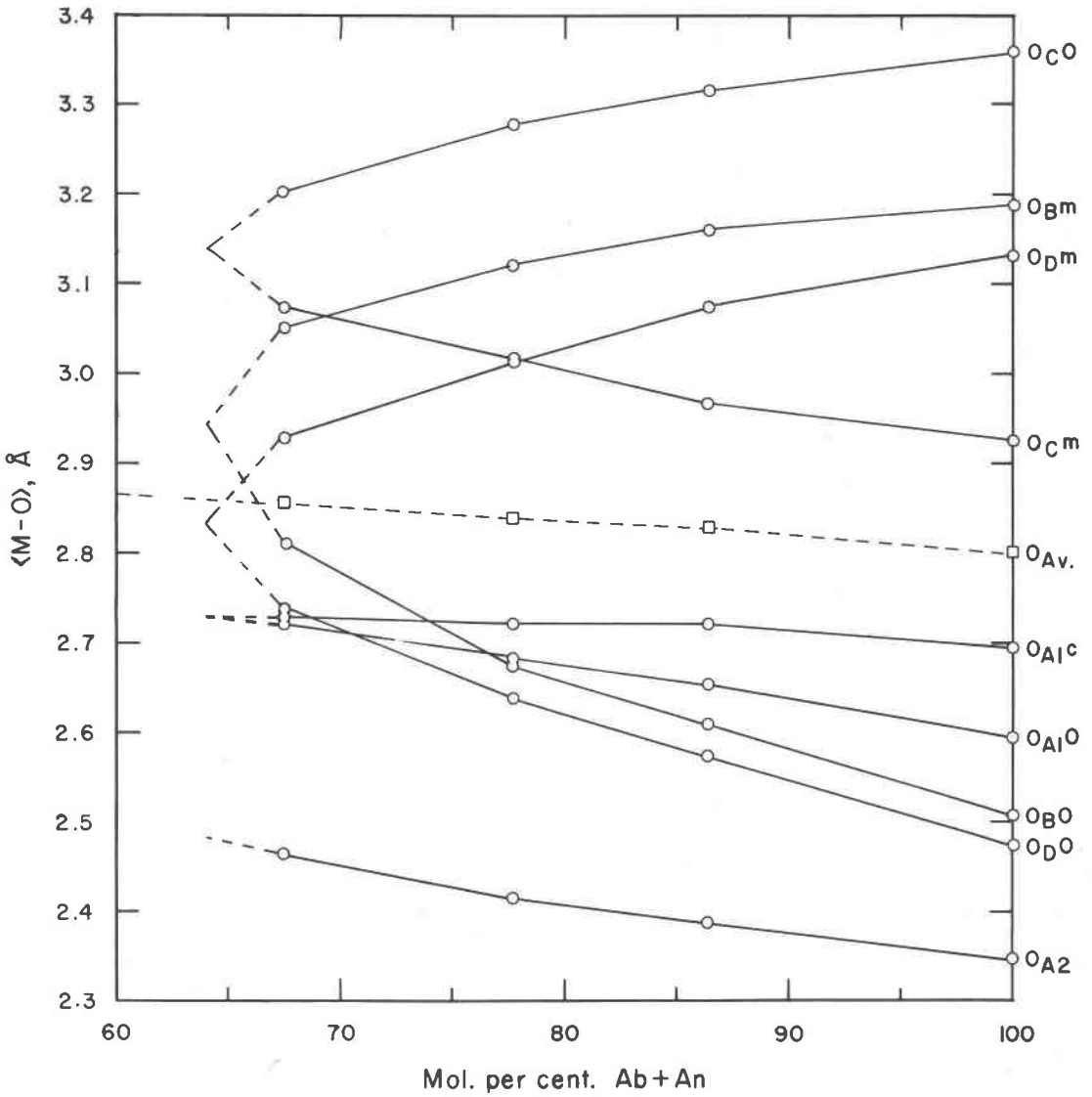

Fig. 6. The variation of individual M–O distances with composition. The dashed lines represent reasonable extrapolations for a room-temeprature transition to monoclinic symmetry at Or_{36}.

O_Cm bonds. A projection[1] of the M-site coordination for both the room- and high-temperature structures (superimposed) of the Kakanui sample, viewed down the intermediate axis of the thermal expansion "strain" ellipsoid, shows the obvious correlation between the above-mentioned bond distances and the gross expansion of the feldspar structure on heating (Fig. 9). The interlinkage of the framework tetrahedra causes adjustments in the geometry that account for the slight misalignment of the inter-structure site displacements with respect to the cell thermal expansion between the structures. These changes are basically rotations of fixed size tetrahedra. Henderson (1979) suggests that the $M–O_{A2}$ extension with rotation of the framework structure is chiefly responsible for the expansion.

[1]This projection of two structures upon one another requires the choice of a joint reference frame. This frame should not be the one chosen by Ohashi and Burnham (1973) for calculating the strain tensor from an arbitrary deformation tensor, because it includes a rotation produced by constraining the *c* and *a* axes to be parallel for the two lattices. Consequently, the reference frame chosen for the projection is the one for which the deformation tensor relating the two lattices is a symmetric tensor describing a pure strain and no rotation. The amount of rotation is less than 2° for the crystals examined here, but it is still noticeable in the projections if it is not taken into account.

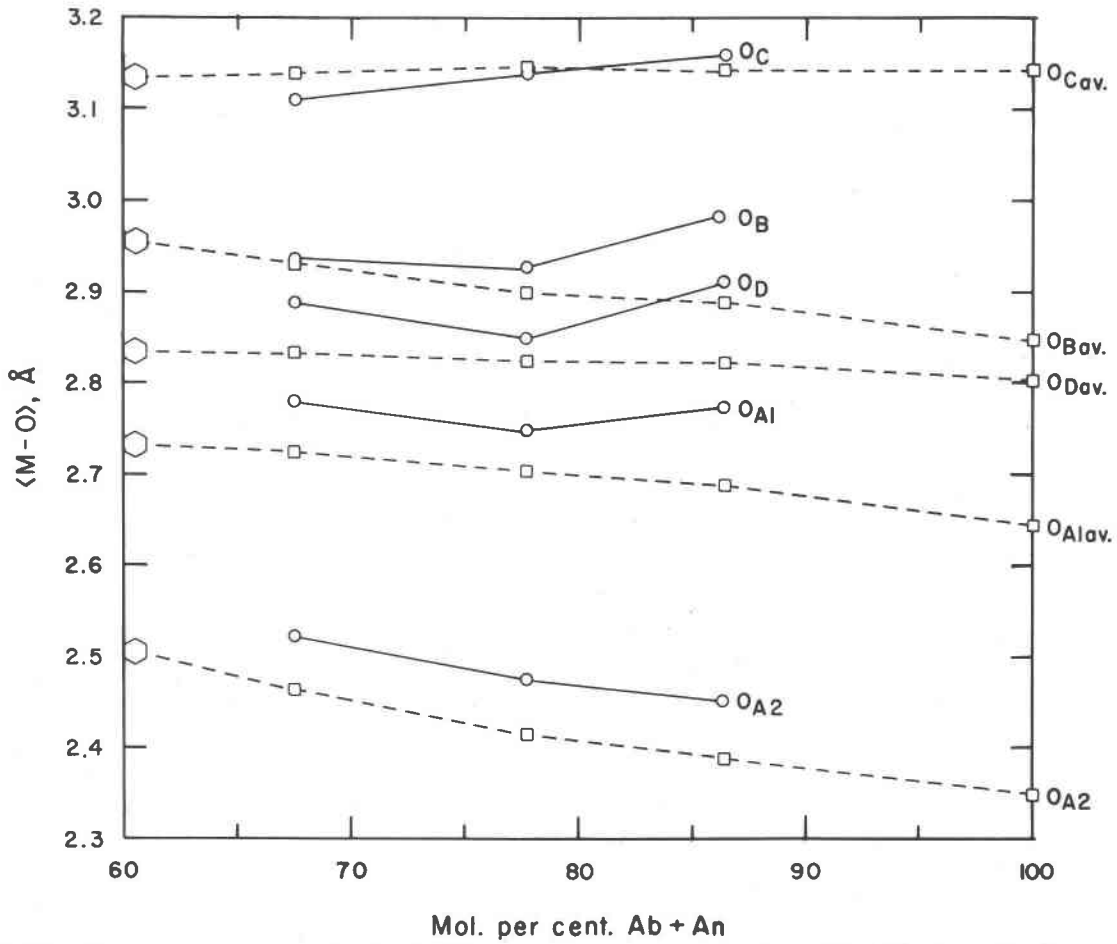

Fig. 7. M–O distances *versus* composition for the high-temperature structures (circles and solid lines) and for the monoclinic averages of the room-temperature structure values (squares and dashed lines). Note the general increase in $M–O_{A1}$, and $M–O_{A2}$, which reflect the M-site cavity width.

Inflation of the cavity is a more accurate cause as other bonds ($M–O_D0$, $M–O_B0$ and $M–O_Cm$) show greater expansion.

T–O–T angles. The T–O–T angles (Table 7) in feldspars are extremely variable and manifest in some degree the compliance of the tetrahedral framework to the lattice geometry determined by the overall nature of the feldspar structure, the degree of "inflation" from bonding effects of alkali atoms in the M-site cavity, and the degree of Si,Al order. Increasing Or content and increasing temperature both decrease the variance in the angles and increase their average value for a single structure, which indicates inflation of the structure and an approach to the ideal monoclinic feldspar structure (*cf.* Megaw, 1974). This relation also means a decrease in triclinicity for the triclinic structures, which is evident on comparing the angles that are equivalent for monoclinic symmetry (*e.g.*, $T–O_B0–T$ *vs.* $T–O_Bm–T$). The difference decreases with increasing Or content, trending to zero on transition to monoclinic symmetry. As in the case of the cell angle, a graphical examination can be helpful in evaluating the composition of the triclinic/monoclinic inversion. The value $\cos^2(\Delta T–O–T)$, where $\Delta T–O–T$ is the difference between pseudosymmetrically related T–O–T angles, was plotted against Or content in Figure 10 in expectation that it would have the same linear relationship as expected for $\cos^2\alpha$ (Thompson *et al.*, 1974). The relationship for each of the differences for O_B, O_C and O_D is very close to linear, extrapolating to values close to Or_{36} (35.8, 35.3 and 35.1, respectively) for a room-temperature inversion, which is consistent with the estimate based on $\cos^2\alpha$.

Apparent thermal motion. The magnitudes of

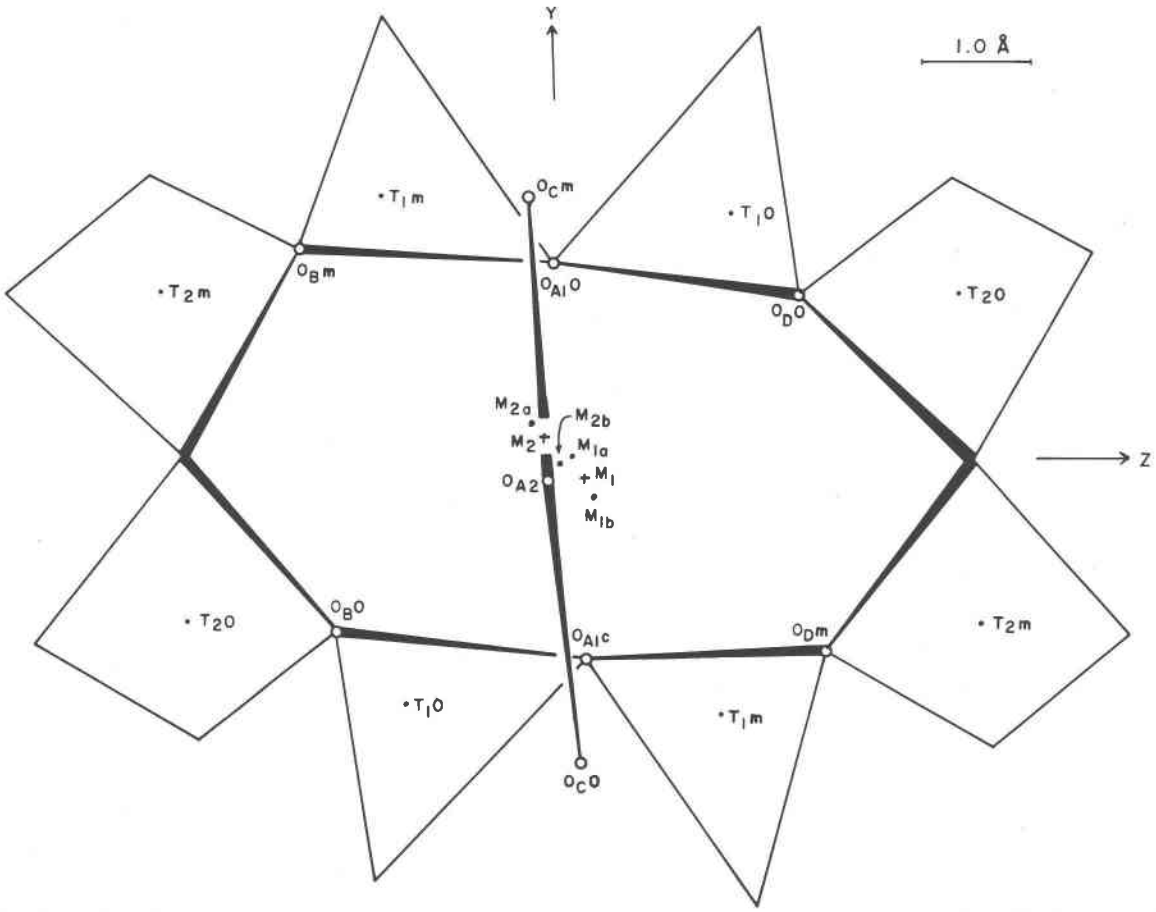

Fig. 8. The M-site coordination for the Mt. Gibele crystal (23°) projected onto the *b*–*c* plane (down *a**) with split sites. Note the elongation in the O_Bm–O_Dm direction and the distribution of the subsites in that direction. O–O tetrahedron edge lines taper to show relative height of site in the projection direction; higher site is at the wide end of the line.

apparent thermal motion (either in terms of equivalent isotropic B or root-mean-square (RMS) displacements) for the room-temperature structures (Table 8) are comparable to those from other disordered feldspars, except perhaps for the large and unusual values for the M-site. On the average, Grande Caldeira, $Or_{32.5}An_{0.8}$ has the lowest temperature factors, Kakanui, $Or_{13.8}An_{2.5}$, has the intermediate, and Mt. Gibele, $Or_{22.3}An_{6.9}$, has the largest. There are several possible reasons for this relationship. First, greater differences in the real positions of the atoms relative to that in the average structure may exist within the respective crystals. The larger temperature factors in crystals with higher An content are caused by large local distortions from extra aluminum in the T sites (Phillips and Ribbe, 1973b) and by the stronger bonding of Ca in the M-site. Second, variation in the perfection of the crystals can affect the temperature factors; this can be partially improved with an extinction correction, although such a correction was not attempted. Finally, of course, variation in a systematic error in each data set (such as absorption) can cause decreases in "high angle" diffraction intensities. However, the anorthite content is the most likely controlling factor, and it is significant that the small variations in An content (6 mole%) cause such noticeable effects.

Apparent thermal motion models in high temperature structures are likely to represent an average of real vibrational motion and inter-M-site migration as well as positional disorder because the effect of temperature is to increase atomic and lattice vibrations and alkali diffusion within a feldspar crystal. Magnitudes of equivalent isotropic B's for atoms in the high-temperature refinements are 1.4 to 3.4 times larger than for their room-temperature equivalents. They decrease, in both room-

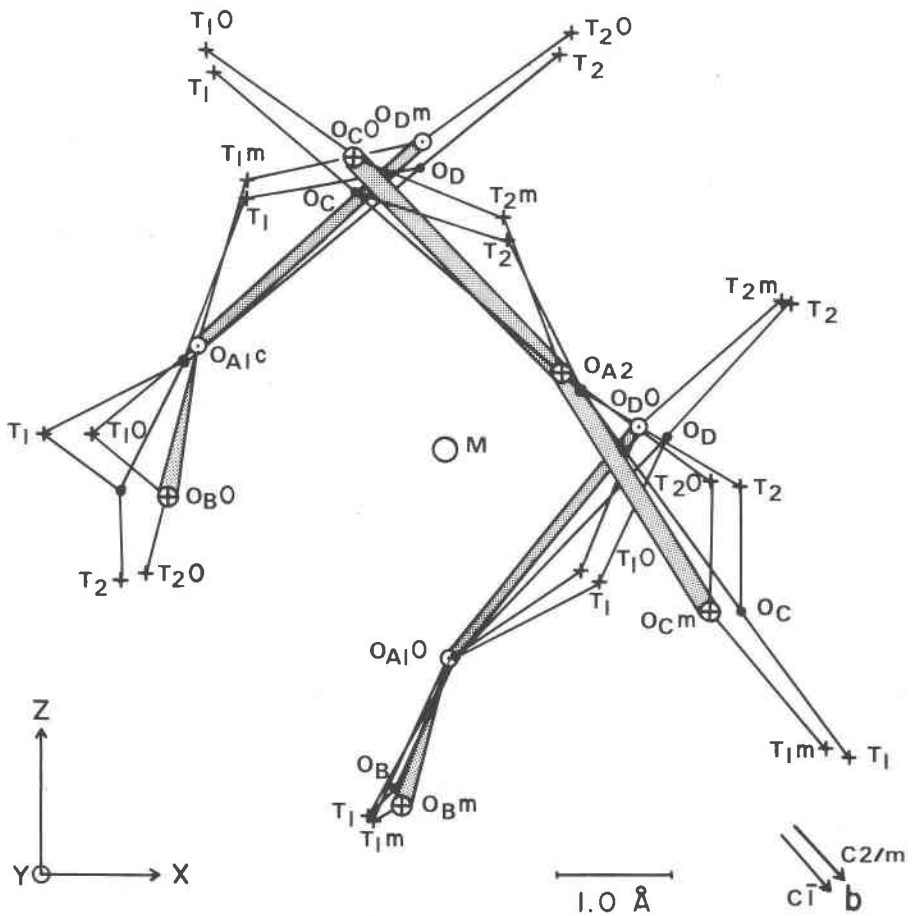

Fig. 9. Projection of the M-site region down the intermediate, *y*, axis of the strain ellipsoid of thermal deformation for the Kakanui crystal. The positions are corrected for rotation as evaluated in the strain analysis (see text). The closest unit cell axis is projected onto the plane of the projection for a reference. Note that the major atomic displacements relative to M are in agreement with the major (*x*) and minor (*z*) axes of strain suggesting the importance of M–O bonding on thermal deformation. O–O lines taper to show the higher site at wide end of the line.

temperature and high-temperature structures, in the following order: M, O_B, O_{A2}, O_{A2}, O_C, O_D, T_1, T_2. This similarity in ranking indicates either that the relative effects of disorder and real thermal motion are about the same or that real thermal motion dominates the effects observed at both room and high temperatures. However, this may not be a valid conclusion for the M site with its possible splitting. The magnitude of apparent motion for each atom increases with temperature except for Grande Caldeira the most potassic composition. The difference for Grande Caldeira may be related either to the higher Or content or to the crystal perfection of the sample.

The very large thermal ellipsoid for the M site in the room-temperature anorthoclase structures is comparable to that in high albite (Ribbe *et al.*, 1969, and Wainwright, unpublished, see Smith, 1974, Prewitt *et al.*, 1976, Winter *et al.*, 1979) except that the minor axis is always negative, causing the thermal models to be unreal. The thermal parameters of the M-site cations are highly correlated with alkali chemistry and temperature. Both equivalent B and the major axis displacement of the thermal ellipsoid increase with decreasing Or content and increasing temperature. Ellipsoid orientations for the room-temperature structures have a consistent orientation with the unreal (negative) axis parallel to a^* and the short M–O_{A2} bond and with the major axis oriented subparallel to the cavity elongation in the *b*–*c* plane (Fig. 8, compare with Fig. 9a of Winter *et al.*, 1979). These orientations are controlled by the shorter M–O bonds (M–O_{A1} and M–O_{A2}) and the general triclinic distortion of the cavity. In the monoclinic structures the cavity is symmetrically constrained to be elongated parallel

Table 7. T–O–T angles

	Grande Caldeira			Mt. Gibele			Kakanui		
	23°	23° C2/m Average	400°	23°	25° C2/m Average	510°	23°	23° C2/m Average	750°
O_{A1}	143.5(2)	143.5	144.4(5)	143.8(2)	143.8	143.3(3)	143.6(2)	143.6	141.9(7)
O_{A2}	132.2(2)	132.2	135.1(5)	130.8(2)	130.8	132.5(3)	130.5(2)	130.5	133.7(5)
O_B0	148.8(2)	151.6	150.7(4)	145.2(2)	150.7	150.9(2)	143.5(2)	150.6	153.2(4)
O_Bm	154.4(2)			156.2(2)			157.8(2)		
O_C0	132.1(2)	132.7	131.9(3)	131.8(2)	132.8	133.2(2)	131.2(2)	132.7	136.1(4)
O_Cm	133.3(2)			133.8(2)			134.2(2)		
O_D0	139.8(2)	142.0	142.6(3)	137.9(2)	142.3	142.1(2)	136.5(2)	141.5	145.4(4)
O_Dm	144.2(2)			146.7(2)			148.4(2)		
Average	141.32		141.57	141.11		141.29	140.81		142.99
σ of Av.	7.76		7.19	8.27		7.09	9.03		7.11

Estimated standard deviations in parenthese refer to the last digits

to the *b* axis; the major axis for the M-site also lies in this direction, about 37° from that at room-temperature (see also Fig. 9b of Winter *et al.*, 1979).

M-site modeling. Fourier sections through the M site show a very compact electron density distribution in the *a** direction and a very elongate distribution in the *b*–*c* plane. Though the distributions appear ellipsoidal in shape, they are evidently not statistically normal with respect to electron density distributions as a function of distance from the centroid. The electron density distribution in the *a** direction is apparently more peaked than the combined X-ray scattering form-factors (when elliptically displaced from the centroid in the plane normal to *a**) for the averaged M-site occupants. Use of extended cumulant approximations (higher order real-space tensors) to allow for the skewness and kurtosis of the scattering power distribution (Johnson, 1969) do not adequately improve the refinements nor eliminate the negative ellipsoid axis.

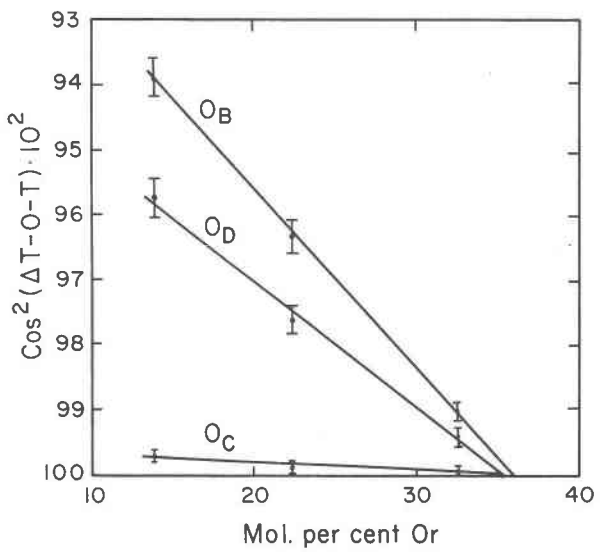

Fig. 10. Plot of $\cos^2(\Delta T\text{–}O\text{–}T)$ angle (difference in pseudosymmetrically equivalent angles, *e.g.* for O_B0 and O_Bm) *vs.* composition of the 23° C anorthoclase structures. Best fit lines determined by least squares extrapolate to transition composition near Or_{36}.

The large magnitudes of apparent thermal vibration for the M-site cation, 0.27 to 0.40Å maximum RMS amplitude, are considered too large to be purely vibrational in nature and may be in part due to displacement of individual alkali atoms into one of several subsites. In the case of high albite, Ribbe *et al.* (1969) developed a model based on a split M-site, with the site being divided into four separate quarter-atom sites, based on an analogy with anorthite which has a similar structure. Winter *et al.* (1979) looked at other possibilities of multiple subsites for high albite and monalbite in relation to low albite. The three room-temperature data sets described in this paper were refined with various M subsites to examine the applicability of such models. The following models proved to be the best of the many ones attempted, based on Hamilton's (1965) crystallographic *R* factor comparison; the unreal anisotropic solution is used as a reference (see Table 9). For the two most Na-rich anorthoclases, the best model consists of four positionally

Table 8. Thermal ellipsoids—RMS displacements and angles to cell axes

	RMS Displacements (Å)			Angles to Cell Axes (°)									
				Axis 1			Axis 2			Axis 3			B equiv.
	1	2	3	a	b	c	a	b	c	a	b	c	
Grande Caldeira 23°													
T_1O	0.098(2)	0.112(2)	0.131(2)	117(5)	103(6)	12(6)	116(4)	141(5)	100(7)	40(4)	126(4)	95(4)	1.04(1)
T_1m	0.098(2)	0.104(2)	0.131(2)	126(7)	67(12)	27(15)	109(9)	46(10)	116(15)	42(3)	53(3)	95(4)	0.99(1)
T_2O	0.095(2)	0.117(3)	0.120(3)	95(5)	172(5)	81(5)	77(32)	97(5)	164(26)	14(30)	93(5)	103(32)	0.98(1)
T_2m	0.095(2)	0.113(3)	0.123(2)	79(4)	169(4)	93(6)	70(11)	87(6)	173(10)	23(10)	79(3)	96(11)	0.98(1)
M	0.063 (6)	0.139(5)	0.272(3)	26(2)	91(2)	91(2)	70(2)	125(1)	144(1)	105(1)	145(1)	54(1)	2.36(4)
O_{A1}	0.131(5)	0.157(5)	0.188(4)	114(5)	92(10)	2(6)	104(5)	14(6)	89(10)	28(5)	76(6)	92(5)	2.03(4)
O_{A2}	0.125(5)	0.150(3)	0.177(4)	88(6)	177(7)	88(5)	128(7)	93(7)	116(7)	142(7)	90(5)	26(7)	1.83(4)
O_BO	0.131(5)	0.185(4)	0.194(5)	153(4)	111(5)	51(5)	103(8)	98(17)	140(5)	67(5)	157(6)	97(15)	2.33(5)
O_Bm	0.133(5)	0.180(4)	0.190(5)	152(4)	68(5)	50(5)	107(7)	87(16)	137(7)	112(6)	158(5)	76(14)	2.28(5)
O_CO	0.135(4)	0.158(4)	0.162(4)	82(9)	18(7)	81(8)	146(54)	75(12)	94(55)	123(55)	99(17)	10(25)	1.83(4)
O_Cm	0.127(4)	0.148(4)	0.174(4)	80(7)	165(8)	82(6)	124(7)	105(8)	117(7)	144(7)	91(6)	28(7)	1.81(4)
O_DO	0.125(5)	0.152(5)	0.174(4)	77(5)	121(7)	49(6)	91(10)	149(7)	116(8)	167(5)	96(9)	52(6)	1.81(4)
O_Dm	0.129(4)	0.158(4)	0.175(4)	75(5)	63(6)	50(5)	111(13)	30(9)	100(10)	154(10)	103(12)	42(5)	1.90(4)
Grande Caldeira 400°													
T_1	0.127(2)	0.159(3)	0.199(2)	122(7)	97(3)	9(3)	100(4)	161(3)	98(3)	34(2)	106(3)	86(2)	2.13(3)
T_2	0.145(2)	0.146(2)	0.194(2)	122(37)	105(72)	17(73)	83(21)	161(73)	108(69)	33(2)	94(3)	83(2)	2.11(3)
M	0.157(10)	0.269(10)	0.302(10)	13(3)	90	103(3)	77(3)	90	167(3)	90	0	90	4.96(16)
O_{A1}	0.123(8)	0.204(8)	0.263(6)	108(2)	90	8(2)	90	0	90	18(2)	90	98(2)	3.32(11)
O_{A2}	0.164(8)	0.198(10)	0.233(9)	90	0	90	73(10)	90	170(10)	17(10)	90	99(10)	3.18(12)
O_B	0.168(5)	0.237(6)	0.259(6)	151(3)	105(5)	41(3)	108(8)	18(5)	85(12)	68(5)	80(18)	49(4)	3.98(10)
O_C	0.174(7)	0.200(6)	0.253(7)	80(10)	13(8)	86(9)	26(7)	95(10)	141(5)	66(5)	102(5)	52(5)	3.53(10)
O_D	0.182(9)	0.218(7)	0.240(6)	80(5)	147(7)	66(8)	71(10)	117(9)	152(9)	21(10)	73(8)	103(8)	3.64(9)
Mt. Gibele 23°													
T_1O	0.103(2)	0.129(2)	0.153(2)	118(3)	109(5)	17(5)	84(3)	160(5)	107(5)	29(3)	94(3)	87(3)	1.33(2)
T_1m	0.104(2)	0.110(5)	0.156(2)	111(12)	106(19)	14(21)	119(8)	29(12)	76(21)	38(2)	66(2)	88(2)	1.25(2)
T_2O	0.102(2)	0.125(5)	0.151(2)	88(4)	167(4)	78(6)	55(4)	99(5)	165(5)	36(4)	81(2)	83(4)	1.28(2)
T_2m	0.102(2)	0.120(5)	0.155(2)	83(5)	165(4)	78(7)	58(4)	98(7)	168(7)	33(3)	77(2)	86(4)	1.29(2)
M	0.019 (5)	0.090(8)	0.319(3)	20(3)	99(4)	98(5)	81(7)	127(2)	139(2)	107(1)	142(1)	50(1)	2.89(5)
O_{A1}	0.132(5)	0.166(5)	0.211(4)	113(6)	102(8)	10(9)	67(4)	157(5)	100(9)	34(5)	71(4)	89(4)	2.53(5)
O_{A2}	0.123(5)	0.171(4)	0.184(4)	87(4)	170(4)	81(5)	83(20)	99(5)	157(19)	7(18)	86(5)	110(20)	2.06(5)
O_BO	0.150(5)	0.192(4)	0.202(4)	147(6)	103(7)	35(5)	112(10)	26(15)	94(10)	68(9)	68(16)	55(5)	2.64(6)
O_Bm	0.145(4)	0.190(5)	0.203(4)	151(4)	69(6)	47(6)	98(7)	61(14)	137(7)	62(4)	37(11)	84(12)	2.59(6)
O_CO	0.148(5)	0.163(4)	0.182(4)	103(14)	22(19)	71(18)	55(12)	68(19)	157(19)	38(13)	90(7)	78(13)	2.15(5)
O_Cm	0.136(5)	0.164(4)	0.189(7)	76(5)	163(5)	84(8)	92(10)	101(8)	148(10)	166(5)	103(5)	59(10)	2.14(5)
O_DO	0.139(5)	0.161(5)	0.193(6)	87(6)	126(9)	43(9)	80(8)	143(9)	125(8)	11(8)	80(7)	113(7)	2.17(5)
O_Dm	0.154(5)	0.154(5)	0.192(7)	90(180)	67(180)	36(180)	104(58)	19(180)	97(180)	166(7)	103(7)	59(6)	2.23(5)
Mt. Gibele 510°													
T_1	0.130(2)	0.143(2)	0.177(2)	124(7)	105(3)	18(7)	113(9)	138(6)	107(8)	43(6)	127(8)	92(2)	1.76(2)
T_2	0.132(4)	0.149(3)	0.158(2)	79(6)	11(6)	90(5)	53(8)	92(4)	168(8)	39(7)	101(10)	78(12)	1.70(2)
M	0.128(6)	0.259(4)	0.301(4)	20(2)	90	95(3)	69(3)	90	174(3)	90	0	90	4.59(7)
O_{A1}	0.147(6)	0.218(6)	0.239(5)	112(5)	90	3(5)	90	180	90	23(5)	90	93(5)	3.33(8)
O_{A2}	0.156(6)	0.184(6)	0.229(5)	90	0	90	143(9)	90	100(9)	126(9)	90	10(9)	2.91(7)
O_B	0.149(4)	0.238(4)	0.260(4)	159(4)	107(3)	53(4)	89(4)	127(8)	136(5)	69(16)	137(10)	69(11)	3.86(6)
O_C	0.162(5)	0.210(4)	0.230(4)	66(8)	25(9)	93(3)	154(9)	65(9)	72(8)	98(8)	95(4)	18(8)	3.24(6)
O_D	0.165(4)	0.224(4)	0.232(4)	76(7)	111(4)	45(4)	109(34)	154(35)	95(18)	155(32)	76(14)	45(32)	3.45(6)
Kakanui 23°													
T_1O	0.105(2)	0.117(2)	0.136(2)	33(8)	61(5)	101(9)	63(9)	114(6)	154(5)	73(4)	141(3)	66(4)	1.14(2)
T_1m	0.102(2)	0.116(2)	0.131(2)	153(5)	67(4)	55(5)	111(6)	109(5)	127(5)	105(4)	149(5)	56(5)	1.08(2)
T_2O	0.104(2)	0.114(2)	0.134(2)	54(8)	44(8)	87(4)	140(7)	50(7)	73(5)	105(5)	106(4)	17(5)	1.10(2)
T_2m	0.109(2)	0.110(2)	0.133(2)	19(110)	108(129)	109(22)	105(133)	154(98)	98(43)	100(4)	108(4)	21(4)	1.10(2)
M	0.068 (5)	0.095(11)	0.397(3)	30(3)	89(2)	86(3)	65(4)	127(1)	140(1)	107(1)	143(1)	50(1)	4.27(8)
O_{A1}	0.143(4)	0.167(5)	0.179(4)	120(8)	75(10)	19(9)	117(13)	152(13)	76(12)	43(13)	112(15)	79(8)	2.12(5)
O_{A2}	0.134(5)	0.146(4)	0.165(4)	60(12)	34(14)	94(9)	126(12)	59(15)	109(11)	130(9)	79(9)	20(10)	1.75(4)
O_BO	0.132(5)	0.170(4)	0.193(4)	161(5)	108(7)	57(6)	80(8)	138(7)	127(7)	74(4)	126(7)	54(7)	2.20(5)
O_Bm	0.124(5)	0.178(4)	0.210(4)	161(4)	75(4)	55(4)	107(4)	120(6)	125(5)	97(3)	146(5)	54(5)	2.40(5)
O_CO	0.131(5)	0.150(5)	0.187(4)	57(11)	41(10)	87(7)	34(10)	124(10)	112(7)	100(6)	109(5)	23(6)	1.97(5)
O_Cm	0.133(4)	0.151(5)	0.175(4)	54(5)	109(9)	65(6)	89(9)	156(10)	109(10)	144(5)	105(9)	33(6)	1.88(4)
O_DO	0.134(4)	0.156(5)	0.174(4)	60(5)	100(7)	56(5)	83(11)	164(12)	103(12)	149(6)	102(13)	37(6)	1.91(5)
O_Dm	0.121(4)	0.166(5)	0.195(4)	64(4)	68(4)	59(3)	47(7)	137(7)	107(7)	125(6)	125(7)	37(5)	2.11(5)
Kakanui 750°													
T_1	0.163(5)	0.198(3)	0.222(3)	135(3)	100(4)	22(4)	123(4)	120(4)	112(4)	63(4)	148(4)	88(4)	3.04(5)
T_2	0.176(4)	0.195(3)	0.206(2)	170(8)	99(9)	59(5)	83(10)	167(8)	102(9)	83(4)	99(12)	34(6)	2.93(5)
M	0.189(6)	0.388(11)	0.459(12)	25(2)	90	91(2)	65(2)	90	179(2)	90	0	90	10.4(4)
O_{A1}	0.223(9)	0.266(11)	0.305(6)	110(4)	90	6(4)	90	180	90	20(4)	90	96(4)	5.6(2)
O_{A2}	0.196(8)	0.217(10)	0.374(14)	35(3)	90	81(3)	90	180	90	125(3)	90	9(3)	5.9(3)
O_B	0.175(17)	0.297(5)	0.334(10)	157(4)	107(4)	50(3)	107(5)	88(10)	136(5)	105(4)	17(5)	76(9)	6.1(2)
O_C	0.211(11)	0.278(11)	0.289(6)	58(6)	33(6)	100(6)	34(13)	120(8)	125(30)	80(26)	100(17)	37(30)	5.4(2)
O_D	0.228(8)	0.262(12)	0.292(9)	85(8)	115(9)	39(10)	51(12)	133(10)	127(10)	39(11)	53(10)	99(9)	5.4(2)

* $i = \sqrt{-1}$ for this imaginary displacement of the non-positive definite ellipsoid

Estimated standard deviations in parentheses refer to the last digits

Table 9. Results of refinements of multi-site models for the M site

Grande Caldeira 23°	R_w	R_u	R	Signif. Level %	Occup.	X	Y	Z	B Equiv.	Major Splitting
Anisotropic	0.0351	0.0488			1.0	0.2750(2)	0.0013(2)	0.1366(2)	2.36(6)	
Two Subsites	0.0406	0.0546			0.457(29)	0.2749(6)	0.9861(9)	0.1565(12)	0.99(13)	0.43(2)
					0.543	0.2749(5)	0.0130(7)	0.1214(10)	0.67(11)	
Split Species 1	0.0327	0.0412	1.076	>99.5	0.675(Na-Ca)	0.2750(2)	0.0013(1)	0.1365(2)	7.20(16)	
					0.325(K)	0.2750	0.0013	0.1365	2.46(8)	
Split Species 2	0.0318	0.0400	1.106	>99.5	0.675(Na-Ca)	0.2815(7)	0.0005(5)	0.1410(10)	7.15(16)	0.10(1)
					0.325	0.2681(8)	0.0018(3)	0.1324(8)	2.39(7)	
		RMS Displacements (Å) of Na-Ca Site 1: 0.089(8) 2: 0.248(8) 3: 0.450(5) C = 0.56 → General								
Mt. Gibele 23°										
Anisotropic	0.0406	0.0469			1.0	0.2743(2)	0.0033(2)	0.1353(3)	2.89(5)	
Two Subsites	0.0439	0.0536			0.518(18)	0.2731(5)	0.9890(5)	0.1559(8)	0.63(11)	0.51(1)
					0.482	0.2757(5)	0.0191(6)	0.1126(9)	0.66(11)	
Four Subsites	0.0400	0.0460	1.014	>99.5	0.25	0.2734(24)	0.0056(23)	0.1437(26)	0.0	
					0.25	0.2770(10)	0.9773(5)	0.1715(16)	0.76(11)	0.86(2)
					0.25	0.2808(10)	0.0286(5)	0.1001(15)	0.76	
					0.25	0.2697(24)	0.0018(23)	0.1261(25)	0.0	
Split Species 1	0.0404	0.0466	1.005	>99.5	0.777(Na-Ca)	0.2743(2)	0.0033(2)	0.1353(3)	4.27(13)	
					0.223(K)	0.2743	0.0033	0.1353	7.26(55)	
Split Species 2	0.0402	0.0467	1.008	>99.5	0.777(Na-Ca)	0.2733(5)	0.0033(5)	0.1360(8)	3.96(11)	0.07(3)
					0.223(K)	0.2805(23)	0.0028(16)	0.1326(30)	8.46(53)	
		RMS Displacements (Å) of Na-Ca Site 1: 0.085(7) 2: 0.129(10) 3: 0.356(4) C = 0.84 → Prolate								
Kakanui 23°										
Anisotropic	0.0516	0.0579			1.0	0.2743(2)	0.0051(2)	0.1350(3)	4.27(8)	
Two Subsites	0.0599	0.0709			0.501(12)	0.2731(5)	0.9883(5)	0.1604(7)	0.76(10)	0.59(1)
					0.499	0.2752(5)	0.0221(5)	0.1094(7)	0.73(10)	
Three Subsites	0.0519	0.0586			0.218(7)	0.2783(10)	0.9711(9)	0.1816(14)	0.22(4)	
					0.481(7)	0.2710(5)	0.0026(6)	0.1391(10)	0.22	1.00(2)
					0.301	0.2791(7)	0.0308(6)	0.0977(10)	0.22	
Four Subsites	0.0512	0.0572	1.007	>99.5	0.25	0.2697(13)	0.0059(9)	0.1504(12)	0.0	
					0.25	0.2777(8)	0.9734(5)	0.1763(10)	0.22(8)	1.00(2)
					0.25	0.2802(8)	0.0347(5)	0.0972(10)	0.22	
					0.25	0.2725(13)	0.0047(10)	0.1185(12)	0.0	
Grande Caldeira 400°										
Anisotropic	0.0430	0.0728			1.0	0.2796(5)	0.0	0.1366(7)	4.96(16)	
Two Subsites	0.0460	0.0758			0.5	0.2791(6)	0.0148(6)	0.1356(7)	3.59(13)	0.38(1)
Three Subsites	0.0439	0.0748			0.644(53)	0.2812(11)	0.0	0.1500(26)	2.54(22)	
					0.178	0.2755(22)	0.0310(29)	0.1017(38)	2.77	0.81(3)
Split Species 1	0.0423	0.0686	1.017	>99.5	0.675(Na-Ca)	0.2797(5)	0.0	0.1368(7)	10.1(1)	
					0.325(K)	0.2797	0.0	0.1368	4.6(3)	
Split Species 2	0.0415	0.0674	1.035	>99.5	0.675(Na-Ca)	0.2889(20)	0.0	0.1352(30)	10.3(6)	
					0.325(K)	0.2688(24)	0.0	0.1365(26)	4.25(22)	0.17(3)
		RMS Displacements (Å) of Na-Ca Site 1: 0.18(1) 2: 0.38(1) 3: 0.46(2) C = 0.29 → Oblate								
Mt. Gibele 510°										
Anisotropic	0.0343	0.0467			1.0	0.2780(3)	0.0	0.1372(4)	4.59(7)	
Two Subsites	0.0413	0.0592			0.5	0.2780(4)	0.0156(4)	0.1370(5)	3.38(10)	0.40(2)
Three Subsites	0.0373	0.0544			0.327(32)	0.2806(14)	0.0	0.1735(35)	2.17(11)	
					0.336	0.2767(8)	0.0204(7)	0.1190(18)	2.17	0.53(3)
Four Subsites	0.0354	0.0505			0.25	0.2707(19)	0.0	0.0944(20)	1.71(11)	
					0.25	0.2774(21)	0.0	0.1732(22)	1.71	
					0.25	0.2819(17)	0.0259(5)	0.1401(14)	1.71	0.67(2)
Split Species 1	0.0336	0.0454	1.020	>99.5	0.777(Na-Ca)	0.2780(3)	0.0	0.1371(4)	7.90(27)	
					0.223(K)	0.2780	0.0	0.1371	4.62(39)	
Split Species 2	0.0326	0.0437	1.051	>99.5	0.777(Na-Ca)	0.2862(8)	0.0	0.1418(14)	7.84(23)	0.20(3)
					0.223(K)	0.2591(21)	0.0	0.1267(24)	4.18(25)	
		RMS Displacements (Å) of Na-Ca Site 1: 0.154(9) 2: 0.338(9) 3: 0.400(7) C = 0.25 → Oblate								
Kakanui 750°										
Anisotropic	0.0221	0.1047			1.0	0.2839(7)	0.0	0.1406(10)	10.4(4)	
Four Subsites	0.0221	0.1094	1.0002	>50.	0.285(22)	0.2776(20)	0.0	0.0792(37)	3.32(18)	
					0.370(25)	0.2804(19)	0.0	0.1664(37)	3.32	
					0.172	0.2944(23)	0.0544(21)	0.1495(30)	3.32	1.41(4)
Five Subsites	0.0210	0.1082	1.055	>99.5	0.193(24)	0.2837(30)	0.0	0.0601(70)	3.93(26)	
					0.194(26)	0.2840(34)	0.0	0.2082(86)	3.93	
					0.198(19)	0.2952(21)	0.0516(21)	0.1479(31)	3.93	1.34(5)
					0.218	0.2732(19)	0.0	0.1312(47)	0.5	

Estimated standard deviations in parentheses refer to last digits

independent quarter-atom subsites with partially constrained (two fixed and two refined, but equal) isotropic thermal parameters (B's) and each with a Na/K ratio equal to the overall value. The geometry of subsite positions is essentially the same as that for the high-albite model (Ribbe *et al.*, 1969), with two inner sites close to the centroid for the anisotropic model and two outer sites aligned with the cavity elongation (Fig. 9). The value of B for the inner sites, M_{1a} and M_{2b}, was optimized at 0.0, obviously an unrealistic approximation, but roughly equivalent to a single central site with a cylindrical ellipsoid of electron density distribution. The maximum distance between subsites, M_{1b}–M_{2a}, decreases and unconstrained B's increase with increasing Or content. Models for the most K-rich anorthoclase do not converge in least-squares refinement with more than three M-subsites, and none of these models are an improvement over the anisotropic model.

Considering the difference in the relative mass and ionic radius of potassium and sodium, it is likely that the two cations will behave dissimilarly in intermediate alkali feldspar structures as was found by De Pieri and Quareni (1973) and Fenn and Brown (1977). The smaller sodium should be more free to vibrate or rattle in the expanded cavity of an alkali feldspar of intermediate composition, whereas potassium, with its greater mass and radius, should be relatively fixed in the center of the alkali cavity. Thus a model similar to that of De Pieri and Quareni (1973), here called a split-species model, consisting of an isotropic potassium site and an anisotropic sodium (and calcium) site, with occupanices determined by bulk composition, was tested and yielded both a significantly improved *R*-factor and realistic temperature factors (see Table 9). The resulting RMS displacements for the sodium portion of the model are even larger than those for models using a single anisotropic atom and a multiple subsite solution of the sodium site may be indicated. However, no further modeling was attempted. Small differences in the positions of the Na and K subsites are not considered to be significant.

The uniqueness of these multiple partial-atom models is open to debate. Generally the results presented here are comparable to those of Winter *et al.* (1979) for high albite, particularly with respect to sodium anisotropy. They found no compelling reason to accept a static subsite model based on four discrete Si,Al ordering schemes for subsites. In fact, considering the 12 nearest T atoms bonded to the 9 nearest oxygens around the M site of an alkali feldspar, there are 110 configurations which have no Al–O–Al bonds (the aluminum avoidance principle) and have neutral charge (Al:Si = 1.3). This number increases by 390 if ±1 electron/M-site charge is allowed. These possibilities obviously suggest that four discrete domains are unlikely and that local configurations tend to smear out the locus of M sites. Further studies of polarized single-crystal vibrational spectra or a low-temperature structure refinement would be useful in evaluating the nature of the M-site. The data presented here show that the electron distribution is not normal for a single-site model. If thermal vibration is the cause, there is either more than one node to the vibration, *i.e.*, there is some type of positional disorder that may change with time, or the motion is anharmonic. Introduction of potassium into the Na–feldspar structure causes expansion of the average alkali atom cavity so that the sodium may reach greater displacements (either thermal or positional) from the M-site centroid. Also the presence of potassium changes the distribution of electron density such that it is not modelled well by a single averaged atom. Consequently, even more than for the feldspars studied by De Pieri and Quareni (1973), the use of models with separate K and Na(Ca) sites is necessary to achieve a reasonable description of the structures. Splitting of the M-site into many subsites is not demanded but is perhaps reasonable.

In the high-temperature structures the magnitude of apparent thermal motion for the M-site occupant is greater than for the room-temperature structures. The apparent motion is constrained to be symmetric across the (010) mirror plane on which the M site lies, and the delocalization can be adequately described by a real anisotropic model. Thus, there is less reason to attempt models with mutliple partial atoms. However, such modeling was performed to be consistent with the room-temperature results and with the four-site model proposed by Okamura and Ghose (1975) and Prewitt *et al.* (1976) for high albite and the two-site model of Winter *et al.* (1979) for monalbite.

Results of these subsite (averaged alkali atom) models are given in Table 9 and show no measurable improvement over the anisotropic approach. However, the subsite modeling does suggest there is less delocalization of electrons (fewer subsites) with decreasing temperature and/or increasing Or content (consistent with the room-temperature re-

finements). Also the fact that these multiple partial-atom models do not result in better refinements indicates that the use of displacive disorder is probably not an adequate model in these high-temperature structures.

A large central positive residual on several difference Fourier maps suggested a "split-species" model as used for two room-temperature structures. Thus, a model using an isotropic potassium and an anisotropic sodium (calcium) site was attempted. The refinements produced a significantly better R factor than any other model (Table 9). The resulting anisotropic site for the Na,Ca contribution is slightly less oblate and has a slightly larger anisotropy than the totally-averaged site, with the residuals on the difference Fourier section being noticeably smaller. Consequently, a model involving distinct M-site species with different thermal parameters is reasonable and consistent with the data. M–O bond distances for the split sites in the monoclinic high-temperature structures suggest a distorted five- or six-fold coordination, with the M atoms being displaced towards the ends and sides of the alkali cavity (Table 10).

Conclusions

Refinement of three anorthoclase structures at room-temperature (K–analbites) and at high-temperature (K–monalbites) reveal the following points:

(1) Room-temperature cell parameters indicate a large degree of Si,Al disorder consistent with monoclinic topochemistry. High temperature measurements show that these samples do become metrically monoclinic.

(2) Extrapolations of $\cos^2\alpha$ values predicts Or_{36} as the composition for the displacive transformation to monoclinic symmetry at room temperature, which is comparable to estimates of Bambauer *et al.* (1978), Hovis (1980) and Kroll *et al.* (1980). Extrapolations for $\cos^2(\Delta T\text{–}O\text{–}T)$ yield an equivalent result.

(3) T–O–T angles and M–O distances increase in average value and the variance for the averages decreases with increasing Or content at room temperature. This shows a trend to a more regularly coordinated M-site as in the sanidine structure. At high temperature in K–monalbites, increase in Or content and temperature have similar effects upon the alkali feldspar structure, except that K-rich K–monalbites always have a wider and shorter M-site cavity than Na-rich ones. This feature is due to the strong capacity of K to expand the average alkali cation cavity.

(4) An increase in apparent-thermal-motion magnitudes is correlated with the addition of An content and is probably a result of increased local displacement of atoms from the average sites due to the influence of added Ca and Al in the feldspar structure.

(5) Anisotropic thermal models of the M site are unreal at room temperature but, similar to the case of high albite (Ribbe *et al.*, 1969, Wainwright in Smith, 1974) and analbite (Winter *et al.*, 1979), maximum apparent motion is parallel to the cavity length and minimum motion is parallel to a^*, the highly constrained direction of M–O_{A2} and M–O_{A1} bonding. Modeling with multiple isotropic partial atoms suggests structures equivalent to that of Ribbe *et al.* (1969) for high albite or Winter *et al.* (1979) for analbite—four M subsites of which two are greatly displaced from the average centroid parallel to the cavity elongation. These models are less applicable as Or content increases and probably represent an average of many local geometric configurations rather than a domain texture. However a "split-species" model, using a separate isotropic site for K and an anisotropic site for Na(Ca), yields real thermal parameters with significantly improved weighted R factors, further sup-

Table 10. M–O distances for models with split M subsites (in Å)

M Subsites	O_{A1}	O_{A2}	O_B	O_C	O_D	Average
Monalbite 980° (Winter et al., 1979)						
Na_1	2.59(2) 2.95(2)	2.44(1)	2.79(2) 3.11(2)	2.91(2) 3.35(2)	2.68(2) 2.99(2)	2.867
Monalbite 980° (Okamura and Ghose, 1975)						
Na_1(m)	2.73(8)	2.51(9)	2.68(9)			
Na_2(m)	2.74(5)	2.51(7)				
Na_3	2.54(5)	2.40(4)	2.71(10)	2.70	2.60(10)	
Mt. Gibele 510°						
M_1(m)	2.73(2)	2.52(2)	2.71(2)	3.18(1)	3.07(2)	2.876
M_2(m)	2.75(2)	2.51(2)	3.13(2)	3.16(2)	2.65(2)	2.878
M_3	2.57(2) 3.00(2)	2.47(2)	2.95(2) 3.16(2)	2.87(1) 3.40(1)	2.68(2) 3.06(2)	2.881
Kakanui 750°						
M_1(m)	2.84(3)	2.48(3)	2.58(4)	3.19(2)	3.38(5)	2.941
M_2(m)	2.81(3)	2.52(4)	3.36(5)	3.21(3)	2.54(5)	2.930
M_3	2.47(3) 3.30(3)	2.46(3)	2.67(3) 3.46(4)	2.59(3)	2.61(3) 3.34(4)	2.863
Split Species						
Grande Caldeira 400°						
Na(Ca)	2.84(1)	2.45(2)	2.92(2)	3.07(1)	2.93(1)	2.899
K	2.73(2)	2.61(2)	2.94(2)	3.16(1)	2.83(1)	2.882
Mt. Gibele 510°						
Na(Ca)	2.80(1)	2.41(1)	2.95(1)	3.10(1)	2.87(1)	2.871
K	2.65(2)	2.61(2)	2.89(2)	3.23(2)	2.83(2)	2.865

Estimated standard deviations in parentheses refer to the last digits

porting the conclusions of De Pieri and Quareni (1973) and Fenn and Brown (1977) on the different nature of K and Na in intermediate alkali feldspars. Nonetheless, the large anisotropy and displacement magnitudes of the Na(Ca) portion of the site suggest positional disorder as in high albite or analbite for these refinements. For the high-temperature structures multiple partial-atom sites do not provide improvement in modeling of the M-site over an anisotropic apparent thermal motion model. "Split-species" models for the more potassic crystals yield a better match to the data than the other approach, but do not yield the same degree of improvement as found in the room-temperature structures.

Acknowledgments

I want to thank Gordon E. Brown, James B. Thompson, Jr. and the late David R. Waldbaum for stimulating my interest in the feldspars in general and this topic in particular. I am indebted to Eric Dowty and Dan Appleman who offered support and criticism throughout the project. This paper was benefitted from the thoughtful reviews and suggestions of Drs. Hans-Ulrich Bambauer, Maryellen Cameron, Phillip Fenn and Herbert Kroll. This research was supported by National Science Foundation Grant NSF-DES-00527 (Eric Dowty, Principal Investigator).

References

Albee, A. L. and Ray, L. (1970) Correction factors for electron microanalysis of silicates, oxides, carbonates, phosphates and sulphates. Analytical Chemistry, 42, 1408–1414.

Bambauer, H. U., Kroll, H. and Schirmer, U. (1978) Phase transformations and thermal expansion of synthetic, sodium-rich alkali feldspars (c). (Abst. for 1978 IMA Cong.). Physics and Chemistry of Minerals, 3, 5–7.

Bence, A. E. and Albee, A. L. (1968) Empirical correction factors for the electron microanalysis of silicates and oxides. Journal of Geology, 76, 382–403.

Boudette, E. L. and Ford, A. D. (1966) Physical properties of anorthoclase. American Mineralogist, 51, 1374–1387.

Brown, G. E., Hamilton, W. C. and Prewitt, C. T. (1974) Neutron diffraction study of Al/Si ordering in sanidine: a comparison with X-ray diffraction data. In W. S. MacKenzie and J. Zussman, Eds., The Feldspars, p. 68–80. Manchester University Press, Manchester.

Brown, G. E., Sueno, S. and Prewitt, C. T. (1973) A new single-crystal heater for the precession camera and four-circle diffractometer. American Mineralogist, 58, 698–704.

Burnham, C. A. (1962) Lattice constant refinement. Carnegie Institution of Washington Year Book, 61, 132–135.

Carmichael, I. S. E. and MacKenzie, W. S. (1964) The lattice parameters of high-temperature triclinic sodic feldspars. Mineralogical Magazine, 33, 949–962.

Cromer, D. T. and Waber, J. T. (1965) Scattering factors computed from relativistic Dirac-Slater wave functions. Acta Crystallographica, 18, 104–109.

Dal Negro, A., De Pieri, R., Quareni, S. and Taylor, W. H. (1978) The crystal structures of nine K feldspars from the Adamello massif (northern Italy). Acta Crystallographica, B34, 2699–2707.

De Pieri, R., Molin, G. and Zollet, R. (1977) Anorthoclases or plagioclases? A problem of nomenclature. Neues Jahrbuch für Mineralogie, Monatshefte, 413–420.

De Pieri, R. and Quareni, S. (1973) The crystal structure of an anorthoclase: an intermediate alkali feldspar. Acta Crystallographica, B29, 1483–1487.

Dickey, J. S. (1968) Eclogitic and other inclusions in the mineral breccia member of the Deborah volcanic formation at Kakanui, New Zealand. American Mineralogist, 53, 1304–1319.

Fenn, P. M. and Brown, G. E. (1977) Crystal structure of a synthetic, compositionally intermediate, hypersolvus alkali feldspar: evidence for Na, K site ordering, Zeitschrift für Kristallographie, 145, 124–145.

Grove, T. L. and Hazen, R. M. (1974) Alkali feldspar unit-cell parameters at liquid-nitrogen temperatures: Low-temperature limits of the displacive transformation. American Mineralogist, 59, 1327–1329.

Grundy, H. D. and Brown, W. L. (1969) A high temperature X-ray study of the equilibrium forms of albite. Mineralogical Magazine, 37, 156–172.

Hakli, A. (1960) On high temperature alkali feldspars of some volcanic rocks of Kenya and northern Tanganyika. Bulletin of the Geological Society of Finland, 188, 99–108.

Hamilton, W. C. (1965) Significance tests on the crystallographic R factor. Acta Crystallographica, 18, 502–510.

Harlow, G. E. (1977) The anorthoclase structures: A room- and high-temperature study. Ph.D. Thesis, Princeton University, Princeton, New Jersey.

Hazen, R. M. (1976) Sanidine: Predicted and observed monoclinic-to-triclinic reversible phase transformation at high pressure. Science, 194, 105–107.

Hazen, R. M. (1977) Temperature, pressure and composition: Structurally analogous variables. Physics and Chemistry of Minerals, 1, 83–94.

Henderson, C. M. B. (1979) An elevated temperature X-ray study of synthetic disordered Na–K alkali feldspars. Contributions to Mineralogy and Petrology, 70, 71–80.

Hovis, G. L. (1980) Angular relations of alkali feldspar series and the triclinic-monoclinic displacive transformation. American Mineralogist, 65, 770–778.

Johnson, C. K. (1969) Addition of higher cumulants to the crystallographic structure-factor equation: A generalized treatment for thermal-motion effects. Acta Crystallographica, A25, 187–194.

Kroll, H. and Bambauer, H. U. (1981) Diffusive and displacive transformation in plagioclase and ternary feldspar series. American Mineralogist 66, 763–769.

Kroll, H., Bambauer, H. U. and Schirmer, U. (1980) The high albite-monalbite and analbite-monalbite transitions. American Mineralogist, 65, 1192–1211.

Laves, R. (1950) The lattice and twinning of microcline and other potash feldspars. Journal of Geology, 58, 548–571.

Luth, W. C., Martin R. F. and Fenn, P. M. (1974) Peralkaline alkali feldspar solvi. In W. S. MacKenzie and J. Zussman, Eds., The Feldspars, p. 297–312. Manchester University Press, Manchester.

MacKenzie, W. W. (1952) The effect of temperature on the symmetry of high-temperature soda-rich feldspars. American Journal of Science, Bowen Volume, 250A, 319–341.

MacKenzie, W. S. and Smith, J. V. (1962) Single crystal X-ray studies of crypto- and micro-perthites. Norsk Geologisk Tidsskriff, 42, No. 2 (Feldspar Volume), 72–103.

Megaw, H. D. (1974) Tilts and tetrahedra in feldspars. In W. S. MacKenzie and J. Zussman, Eds., The Feldspars, p. 87–113, Manchester University Press, Manchester.

Ohashi, Y. and Burnham, C. W. (1973) Clinopyroxene lattice deformations: The roles of chemical substitutions and temperature. American Mineralogist, 58, 843–849.

Ohashi, Y. and Finger, L. W. (1973) Lattice deformations in feldspars. Carnegie Institution of Washington Year Book, 72, 569–573.

Ohashi, Y. and Finger, L. W. (1974) Refinement of the crystal structure of sanidine at 25° and 400°. Carnegie Institution of Washington Year Book 73, 539–544.

Ohashi, Y. and Finger, L. W. (1975) An effect of temperature on the feldspar structure: crystal structure of sanidine at 800°. Carnegie Institution of Washington Year Book, 74, 569–572.

Okamura, F. P. and Ghose, S. (1975) Crystal structure of monalbite at 980° C. (abstr.) Geological Society of America Abstracts, 7, 1218.

Phillips, M. W. and Ribbe, P. H. (1973a) The structures of monoclinic potassium-rich feldspars. American Mineralogist, 58, 263–270.

Phillips, M. W. and Ribbe, P. H. (1973b) The variations in tetrahedral bond lengths in sodic plagioclase feldspars. Contributions to Mineralogy and Petrology, 39, 327–339.

Prewitt, C. T., Sueno, S. and Papike, J. J. (1976) The crystal structures of high albite and monalbite at high temperatures. American Mineralogist, 61, 1213–1225.

Ribbe, P. H., Megaw, H. D., Taylor, W. H., Ferguson, R. B. and Traill, R. J. (1969) The albite structures. Acta Crystallographica, B25, 1503–1518.

Smith, J. V. (1974) Feldspar Minerals, vol. 1, Crystal structure and physical properties. Springer-Verlag, New York.

Stewart, D. B. (1975) Lattice parameters, composition, and Al/Si order in alkali feldspars. In P. H. Ribbe, Ed., Feldspar Mineralogy, Mineralogical Society of America Short Course Notes, vol. II, p. 1–30. Southern Printing Co., Blacksburg, Virginia.

Stewart, D. B. and Wright, T. L. (1974) Al/Si order and symmetry of natural alkali feldspars, and the relationship of strained cell parameters to bulk composition. Bulletin de la Société Francaise de Minéralogie et de Cristallographie, 97, 356–377.

Thompson, J. B., Jr., Waldbaum, D. R. and Hovis, G. L. (1974) Thermodynamic properties related to ordering in end-member alkali feldspars. In W. S. MacKenzie and J. Zussman, Eds., The Feldspars, p. 218–248. Manchester University Press, Manchester.

Winter, J. K. and Ghose, S. (1977) A reinvestigation of the analbite-monalbite transition at high temperature. (abstr.) Transactions of the American Geophysical Union (EOS), 58, 522.

Winter, J. K., Okamura, F. P. and Ghose, S. (1979) High-temperature structural study of albite, monalbite and the analbite→monalbite phase transition. American Mineralogist, 64, 409–424.

Manuscript received, May 29, 1981;
accepted for publication, June 1, 1982.